Neuroscience

Synchronous Ensembles of Hippocampal CA1 Pyramidal Neurons Associated with Theta but not Ripple Oscillations During Novel Exploration

En-Li Chen, Tsai-Wen Chen, Eric R. Schreiter, Bei-Jung Lin

Institute of Neuroscience, National Yang Ming Chiao Tung University, Taipei, Taiwan • Brain Research Center, National Yang Ming Chiao Tung University, Taipei, Taiwan • Janelia Research Campus, Howard Hughes Medical Institute, Ashburn, VA 20147, USA

Reviewed Preprint

Published from the original preprint after peer review and assessment by eLife.

About eLife's process

Reviewed preprint version 1
April 26, 2024 (this version)

Posted to preprint server
April 23, 2024

Sent for peer review
February 7, 2024

Abstract

Synchronous neuronal ensembles play a pivotal role in the consolidation of long-term memory in the hippocampus. However, their organization during the acquisition of spatial memory remains less clear. In this study, we used neuronal population voltage imaging to investigate the synchronization patterns of CA1 pyramidal neuronal ensembles during the exploration of a new environment, a critical phase for spatial memory acquisition. We found synchronous ensembles comprising approximately 40% of CA1 pyramidal neurons, firing simultaneously in brief windows (~25ms) during immobility and locomotion in novel exploration. Notably, these synchronous ensembles were not associated with ripple oscillations but were instead phase-locked to local field potential theta waves. Specifically, the subthreshold membrane potentials of neurons exhibited coherent theta oscillations with a depolarizing peak at the moment of synchrony. Among newly formed place cells, pairs with more robust synchronization during locomotion displayed more distinct place-specific activities. These findings underscore the role of synchronous ensembles in coordinating place cells of different place fields.

eLife assessment

The authors perform voltage imaging of CA1 pyramidal cells in head-fixed mice running on a track while local field potentials (LFPs) are recorded. They suggest that synchronous ensembles of neurons are differentially associated with different types of LFP patterns, namely theta and ripples. However, evidence for the potentially **useful** findings is currently **incomplete** due to major weaknesses in the experimental and analytical approach.

Introduction

The establishment of long-term memory involves the initial acquisition and subsequent consolidation of memory traces, processes intricately connected to the modification of synaptic transmission[1,2]. Synchronous ensembles, characterized by the simultaneous firing of multiple neurons over tens of milliseconds (referred to as population synchrony), play a pivotal role in influencing synaptic plasticity[3–5]. The hippocampus, a crucial region for long-term memory formation[6,7], has been a focal point of synchronous ensemble studies. Within the hippocampus, synchronous ensembles are hypothesized to play roles in reactivating and consolidating labile memory traces[8]. However, their organization during memory acquisition remains less understood.

In the hippocampus, synchronous ensembles among CA1 pyramidal cells (CA1PCs) are predominantly observed during sharp-wave ripples, the brain waves associated with memory consolidation[8–13]. During these events, 10-18% of CA1PCs generate spikes, particularly during offline consummatory behavioral states or sleep[14,15]. These synchronous ensembles are biased toward experience-dependent reactivation, consolidating labile memory traces[16,17]. Furthermore, synchronous ensembles firing action potentials in short windows of 10-30 milliseconds enhance information processing[6] and discriminate distinct behavioral contingencies[18]. Although synchronous ensembles of CA1PCs during offline memory consolidation are well-characterized, their organization during online acquisition of spatial memory, such as when animals enter a new environment and new place cells form, remains unclear.

Previous studies have identified correlated activities among place cells during theta oscillation, where 1-3% of place cells' spikes co-activate in a forward order matching animals' trajectory in the theta cycles when animals' locations overlap in the place fields of these cells[19–21]. Because these place cells fire at distinct theta phases in the same cycle, this coordinated firing operates on the timescale of theta periods (~125ms)[22,23]. Population synchrony on shorter timescales (10-30 ms) is speculated to be reduced by the presence of theta oscillations[22].

The subthreshold membrane voltage (subVm), influenced by synaptic inputs and intrinsic conductances, directly triggers spiking activity[24,25]. Additionally, properties of subVm support the organization of neuronal representation[26]. Although correlated membrane potentials have been proposed to underlie the synchrony of neuronal ensembles[27,28], multicellular recordings of subVms have not yet provided direct experimental evidence. Given the intricate interaction among subVm, spiking, and place cell formation, it is crucial to investigate the temporal relationships of sub-and suprathreshold neuronal activities among CA1PCs during novel exploration.

In this study, we used voltage imaging to investigate the temporal dynamics of sub-and suprathreshold neuronal activities in CA1PCs during novel exploration. We found synchronous ensembles involving approximately 40% of CA1PCs exhibited transient population synchrony and correlated subthreshold membrane potentials when mice ran and stopped in a new maze. Surprisingly, these synchronous ensembles occurred outside ripple episodes and were phase-locked to extracellular and intracellular theta oscillations. Notably, cell pairs with stronger synchronous activities established more distinct place fields that overlapped less. In essence, synchronous ensembles facilitated temporal association among place cells representing diverse features of spatial memory. This plastic network, driven by synchronous ensembles, may contribute to the stabilization of place cells, establishing place fields that effectively tile the environment.

Results

To investigate the temporal relationships between neuronal activities during novel exploration, we simultaneously recorded many neurons as animals explored a new environment for the first time. To achieve this, we employed voltage imaging in conjunction with an air-lifted plastic track that allowed mice to explore an environment while remaining head-fixed under a microscope (**Figure 1A**). To ensure a genuinely novel experience, all pre-training and habituation were performed in a separate room distinct from the one where the imaging experiments were conducted. On the day of imaging, the mice were introduced to the recording room for the first time and initially confined to a specific corner of the track (**Figure 1A** top view). Subsequently, as the imaging session commenced, the confinement was lifted, granting mice the freedom to explore the track while imaging was conducted.

In novel exploration, mice moved at a speed of 8.3±0.9 cm/s during locomotion (speed>3 cm/s) and spent 53±7% and 36±6% of their time in locomotion and immobility (speed<1 cm/s), respectively (n=5 mice). Meanwhile, they completed 10±2.5 laps during the 180-s imaging periods (n=5 mice).

For voltage imaging, we expressed the voltage indicator Voltron2[29] in CA1 pyramidal cells (CA1PCs), allowing us to measure both suprathreshold and subthreshold membrane potentials from multiple CA1PCs (14±4 cells imaged per field of view (mean±s.d.) and, in total, 71 cells imaged from 5 fields of view in 5 mice; **Figure 1B**). Simultaneously, we monitored the animals' positions and speed within the track while recording the local field potential (LFP) from the contralateral side of the hippocampus.

The mean firing rates of cells ranged from 2.3 to 4.3 Hz (25^{th}-75^{th} percentiles) with a median of 3.2 Hz (n=71 cells, Supplementary Figure 1A). Additionally, most CA1PCs exhibited elevated mean firing rates during immobility relative to locomotion, and their firing rates showed a negative correlation with the animals' speed (Supplementary Figure 1B and 1C), consistent with previous research[30].

Synchronous ensembles among many CA1 pyramidal neurons

Figure 1C shows the fluorescence traces of all neurons in a session as an example. Instances of synchronous activity, where many neurons emitted spikes within a narrow time window, were frequently observed (**Figure 1C**). To investigate synchronous activity within the neuronal population, we selected a reference cell and counted the number of spikes across all other cells that were aligned with the spikes of the reference cell. This approach yielded a grand average cross-correlogram (CCG) capable of elucidating the timing of spikes from the reference cell relative to the combined spikes of the rest of the population. Notably, the grand average CCG exhibited heightened spike counts around zero lags, unlike flattened counts calculated from randomly selected cells of different sessions (**Figure 1D** and **1E**). The full width at half maximum (FWHM) of the peak in the grand average CCG measured 23±14 ms (mean±s.d., n=71 cells from 5 sessions; **Figure 1F**), indicating the timescale of the population synchrony. Furthermore, pairwise CCGs of many cell pairs showed significant peaks compared to jittered data (percentage of significant pairs: 63%, median, n=497 pairs, **Figure 1**-figure supplement 1A and 1B). Among pairs with significant peaks, the absolute values of the peak lags ranged from 0.8 to 4.3 ms (25^{th}-75^{th} percentiles) with a median of 2.1 ms, and the FWHM of the peaks ranged from 20 to 46 ms (25^{th}-75^{th} percentiles) with a median of 30 ms (n=315 pairs, **Figure 1**-figure supplement 1C and 1D). These results highlight the synchronous spiking between neurons on the millisecond timescale.

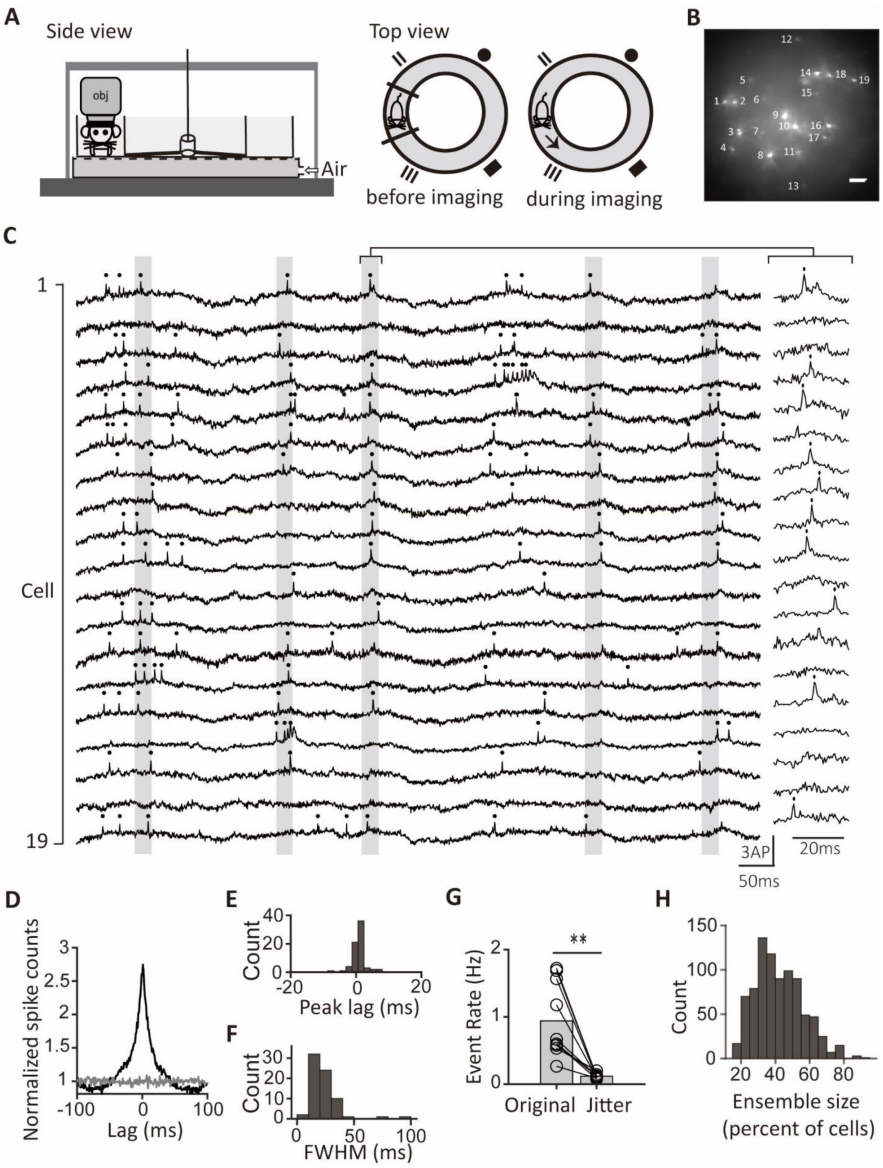

Figure 1

Population synchrony during novel exploration.

(A) Schematic of the behavioral setup for voltage imaging. Mice explored a novel one-way track while fluorescence images were captured at the CA1 pyramidal layer. Left: side view; right: top view of the setup.
(B) Example time-averaged image of CA1 pyramidal cells expressing Voltron2-ST labeled with JF552-HaloTag ligand. Scale bar, 100 ìm.
(C) Fluorescence traces of cells in an example session with identified synchronous ensembles (labeled with gray vertical bars). Right: an example of magnified fluorescence traces within the bracket, pinpointing the occurrence of the identified synchronous ensemble. Spikes are indicated by dots on the top.
(D) The grand average cross-correlogram (CCG) averaged across all 71 cells. The gray line represents the mean grand average CCG between reference cells and randomly selected cells from different sessions.
(E) Distribution of the grand average CCG peak lags of all cells (n=71).
(F) Distribution of the full width at half maximum (FWHM) of the grand average CCGs (n=71 cells).
(G) Pairwise comparison of the event rates of population synchrony between original and jittered data. Bar heights indicate group means. **p<0.01
(H) Histogram of the ensemble sizes as percentages of cells participating in the synchronous ensembles.

To systematically reveal individual synchronous events, we counted the number of spikes from all simultaneously recorded neurons within sliding windows of 25 ms. To compare the summed spikes with controls, we randomly jittered the spike trains to perturb spike timings while maintaining spike rates. We identified moments of population synchrony when spike sums exceeded the average of the jittered spike sums plus four standard deviations (**Figure 1C**). Using the same criterion for event detection, we observed over a 7.8-fold increase in synchronous events in original data compared to jittered controls (mean event rate: 0.94±0.17 Hz for the original data, 0.12±0.01 Hz for the jittered data, n=10 segments, p=0.002, Wilcoxon signed-rank test; **Figure 1G**). Furthermore, we calculated the percentage of neurons participating in these synchronous events to examine the synchronous ensemble sizes. The ensemble sizes ranged from 32% to 53% (25^{th}-75^{th} percentiles) with a median of 42%, which were larger than the synchronous ensemble sizes associated with ripples[14] (**Figure 1H**). These results demonstrate synchronous ensembles of CA1PCs engaging many neurons.

Synchronous ensembles during locomotion and immobility of novel exploration

The hippocampus exhibits state-dependent activities when rodents are engaged in locomotion and immobility[30,31]. In novel exploration, CA1PCs showed synchronous spiking during locomotion and immobility (**Figure 2A**). To investigate whether these synchronous activities differed between these behavioral states, we compared grant average CCGs and synchronous ensembles under these conditions. During both immobility and locomotion, grant average CCGs showed prominent peaks compared to jittered data (**Figure 2B**). Moreover, synchronous ensembles were rich in both immobility and locomotion periods (**Figure 2A**, **2B** and **2D**). Nevertheless, the FWHMs of grant average CCGs were broader in the immobility group compared to the locomotion group (**Figure 2B** and **2C**). Synchronous events occurred more frequently during immobility compared to locomotion (**Figure 2D**). Additionally, ensemble sizes were significantly larger in the immobility group compared to the locomotion group (**Figure 2E**). Taken together, with differences in sizes and kinetics, there were synchronous ensembles during both immobility and locomotion periods of novel exploration.

Synchronous ensembles occur outside ripple episodes

CA1PCs exhibit synchronous activities when the hippocampal network emits ripple waves[8,14]. To test whether there is a co-occurrence of synchronous ensembles and ripples, we first detected ripples from LFP recordings. Ripples were detected in three of the five recording sessions, and all occurred during immobility (mean ripple rate: 0.04±0.02 Hz during immobility, 0 Hz during locomotion). In the two recording sessions where we did not detect any ripples, we verified the recording quality of the LFP signal by running multiple tests after the recording sessions. Ripples were identified in the same animals during quality tests, indicating that the absence of ripples during novel immobility in the recording session was not due to the deterioration of LFP recordings (**Figure 3**-figure supplement 1).

To visualize both ripples and synchronous ensembles, we plotted voltage traces of neurons alongside simultaneously recorded ripple oscillations. It was typical for synchronous ensembles to occur far away from ripple episodes (**Figure 3A**). To delve into the relationship between neuronal activities and ripples, we aligned traces of ripple power with population synchrony and ripples. In a recording session where 64 synchronous ensembles and 12 ripples were detected during immobility, the LFP power at ripple frequency (120-240 Hz) exhibited no discernable peaks within any of the synchronous events (**Figure 3B**, left upper and middle panels). Nevertheless, the same LFP power displayed substantial peaks during every ripple event (**Figure 3B**, right upper and middle panels). A striking contrast between synchronous events and ripples was also evident when spiking probabilities during these events were examined. During population synchrony, the mean spiking probability averaged across all cells was high, while the spiking

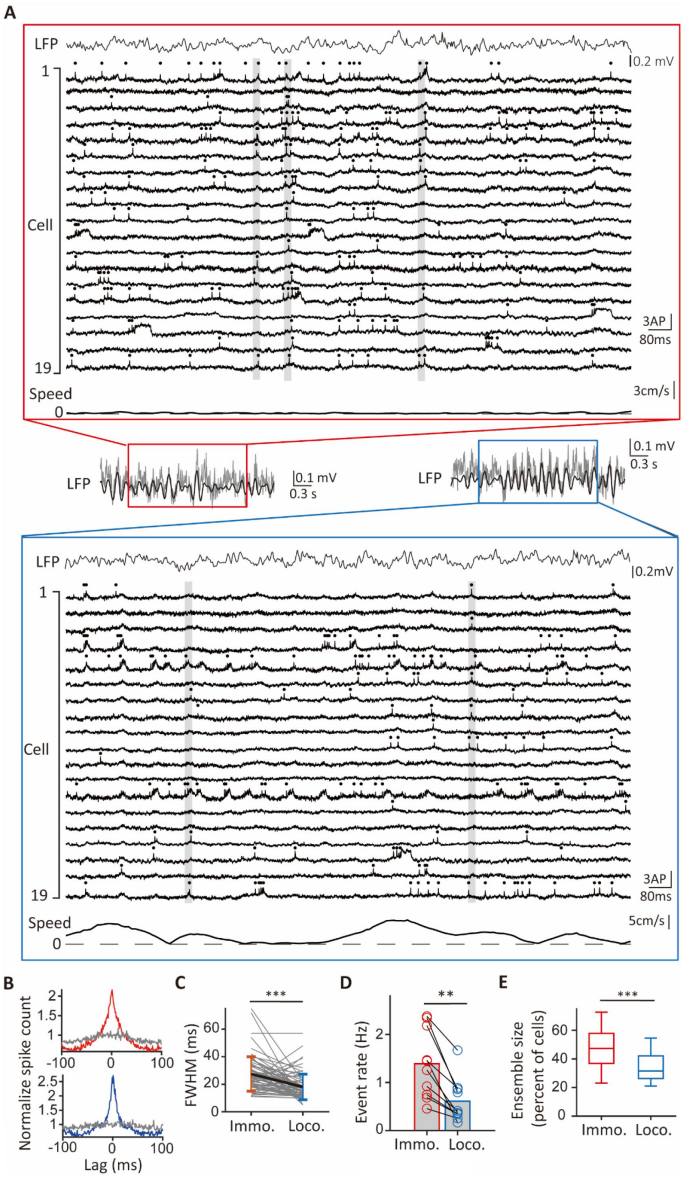

Figure 2

Comparison of synchronous ensembles between immobility and locomotion.

(A) Example traces of cells in a session with identified synchronous ensembles (gray rectangles) during periods of immobility (red rectangular frame) and locomotion (blue rectangular frame). Spikes are indicated by dots at the top of individual traces. Top: the simultaneously recorded LFP trace. Bottom: simultaneously recorded speed of the animal. Inset: the band-pass filtered LFP trace at the theta frequency range (black line) overlaid on the raw LFP trace (gray line).
(B) The grand average cross-correlograms (CCGs) during immobility (red) and locomotion (blue) averaged across all cells (n=71). The gray lines represent the mean grand average CCGs calculated from jittered data.
(C) Pairwise comparison of peak widths (FWHM) in the grand average CCGs between immobility (red) and locomotion (blue). Vertical bars represent means and standard deviations for both groups (FWHM: 27±12 ms for immobility, 18±9 ms for locomotion, mean±s.d., p<0.001, paired Student's t-test, n=71 cells). ***p<0.001
(D) Pairwise comparison of event rates of population synchrony during immobility and locomotion. Bar heights indicate group means (immobility: 1.4±0.7 Hz, locomotion: 0.6±0.5 Hz, mean±s.d., n=10 segments, p=0.002, Wilcoxon signed-rank test). **p<0.01
(E) Boxplot of ensemble sizes for synchronous ensembles occurring during immobility (red) and locomotion (blue) (median ensemble size: 47% for immobility, n=446 events, 32% for locomotion, n=313 events, p<0.001, Wilcoxon rank-sum test). ***p<0.001

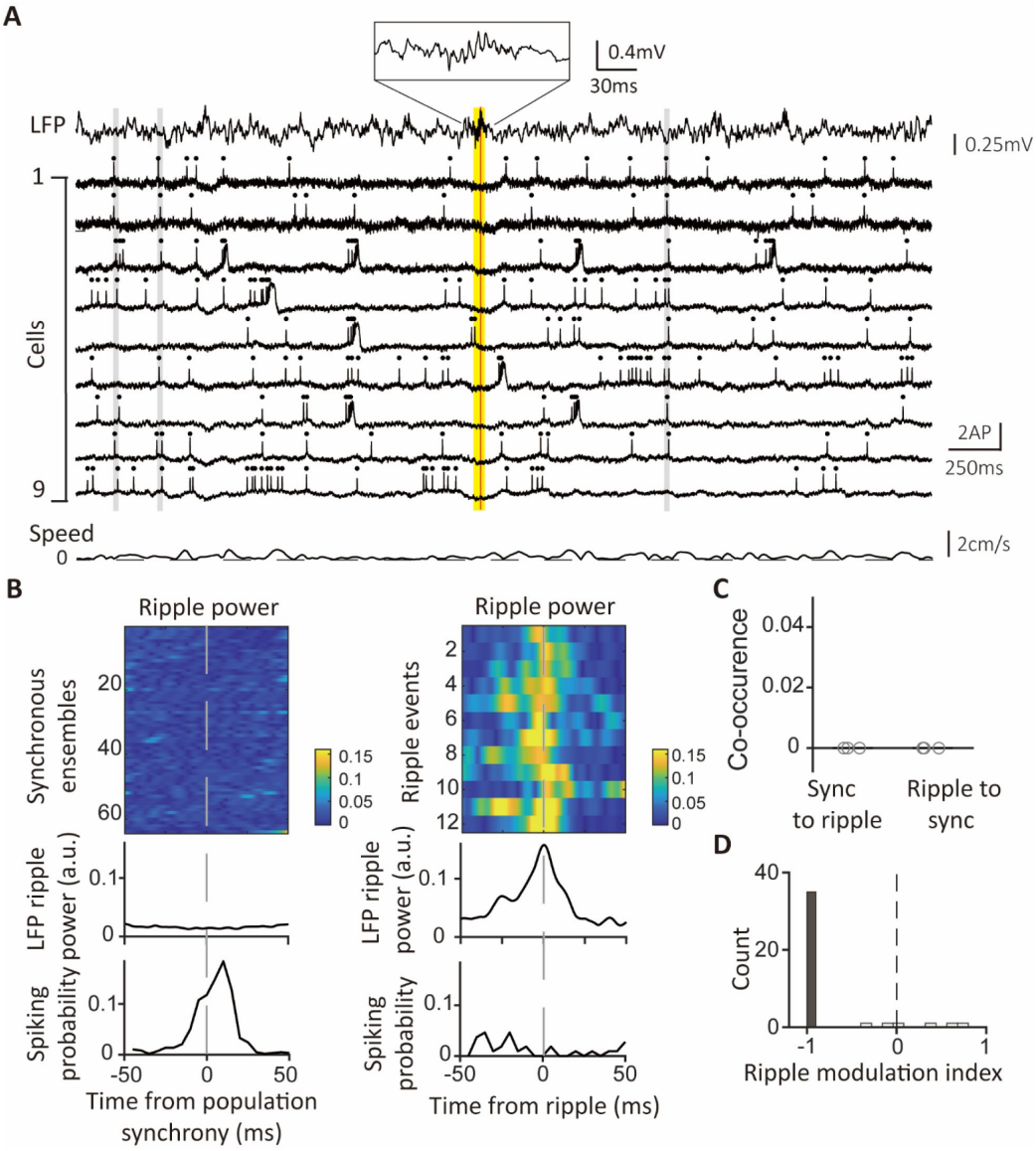

Figure 3

Synchronous ensembles occur outside ripple episodes.

(A) Example traces with ripples and synchronous ensembles. Top: simultaneously recorded LFP displaying an episode of ripple oscillation. A red vertical line indicates the timing of the peak ripple power in the LFP trace. A yellow rectangle marks the duration of the ripple episode. Inset at the top: a magnified view of the ripple oscillation. Middle: fluorescence traces of 9 CA1PCs. Gray rectangles mark the timings of the synchronous ensembles on all traces. Bottom: animals' speed recorded simultaneously with voltage imaging.
(B) LFP ripple power and spiking probability aligned to synchrony ensembles and ripple events. Upper panel: color-coded LFP power at ripple frequency (120-240Hz) aligned to the timings of 64 synchronous ensembles (left) and 12 ripple events (right). Middle panel: Average LFP power of ripple frequency aligned to the timings of the synchronous ensembles (left) and the ripple events (right). Lower panel: Average spike counts of all cells aligned to the timings of the synchronous ensembles (left) and ripple events (right).
(C) Percentages of co-occurrences between population synchrony and ripples. The co-occurrences in the "sync to ripples" group represent the percentages of ripple episodes co-occurring with synchronous ensembles in the same episodes. The co-occurrences in the "ripples to sync" group indicate the percentages of synchronous ensembles co-occurring with ripple episodes. Each gray circle represents an individual session.
(D) Distribution of the ripple modulation indexes (n=41 cells). Gray bar: modulation indexes with significant p values (n=35 cells); white bars: modulation indexes without significance (n=6 cells).

probability was almost zero during ripple events (**Figure 3B** lower panel). In the three sessions where ripples were identified, we calculated the percentages of ripple events coinciding with synchronous ensembles and vice versa. Remarkably, there was no co-occurrence of ripples and synchronous ensembles (**Figure 3C**). Furthermore, we quantified ripple-modulated spiking by calculating the ratio of the difference in mean firing rates during in-ripple and out-ripple periods to the sum of the mean firing rates during both periods. Indexes of most cells were negative, and a striking 85% of cells displayed ripple modulation indexes of-1, indicating complete suppression of their spiking activities during ripples (**Figure 3D**). Taken together, during novel exploration, synchronous ensembles involved many neurons with millisecond-synchronized spikes and occurred outside the time frames of ripples.

Synchronous ensembles are associated with theta oscillations

To investigate the network dynamics associated with synchronous ensembles, we aligned LFP traces triggered by the timings of synchronous ensembles. The average LFP traces of a representative session showed prominent theta oscillations around the timings of both immobility and locomotion population synchrony (**Figure 4A**). Spectral analysis of the mean synchrony-triggered LFP traces during immobility and locomotion revealed theta frequency components of 4-12 Hz, with a slightly higher peak frequency in locomotion LFP compared to immobility LFP (**Figure 4B**). Furthermore, we computed LFP theta modulation and identified preferred phases of synchronous ensembles. In line with the previous result, synchronous ensembles displayed a high level of modulation by LFP theta oscillation (modulation strength: 0.61±0.05 during immobility and 0.74±0.04 during locomotion, n=5 sessions). Although the preferred phases varied from session to session due to differences in recording sites along the proximal-distal axis of the hippocampus, the timings of individual ensembles were consistently locked to the preferred phase of each session (**Figure 4C**). These results establish a strong link between synchronous ensembles and LFP theta oscillation.

Subthreshold membrane voltage (subVm) is one of the critical parameters supporting the generation of action potentials. To investigate the subthreshold signals underlying population synchrony, we aligned subVm traces with the timings of synchronous ensembles and observed that both immobility and locomotion synchrony rode on a subVm waveform oscillating at theta frequency (**Figure 4D**). To elucidate further the relationship between subVm theta oscillation and spikes involved in population synchrony, we calculated the subVm theta modulation and preferred phases of spikes. Spikes participating in both immobility and locomotion synchrony were strongly coupled to the subVm theta oscillation of neurons, with the mean preferred phase being in the latter half of the rising phase closer to subVm theta peaks (**Figure 4E**). Conversely, spikes not participating in synchronous ensembles had weaker modulation strength compared to spikes involved in synchrony (**Figure 4**-figure supplement 1A and 1B). Furthermore, the membrane voltages triggered by these two categories of spikes showed a significant difference in the hyperpolarization phase of the theta oscillation. Synchronous spikes were situated within cycles of theta oscillations featuring more hyperpolarized troughs than spikes outside synchronous ensembles (**Figure 4**-figure supplement 1C and 1D). Thus, compared to spikes not participating in synchronous ensembles, synchronous spikes showed a more robust modulation by theta oscillation of membrane voltage during immobility and locomotion in the context of novel exploration.

Notably, phase locking of spikes to their subVm theta oscillation and the synchronous spikes among many neurons suggest that subVms of different neurons would be correlated at the theta frequency. To explore the possibility, we divided the 180-second subVm traces into 1-second segments with 50% overlap and calculated the cross-correlation and magnitude-squared coherence function for each pair of cell segments. Segments were sorted into the immobility or locomotion group based on the animals' speed during each segment (kept below 1 cm/s for immobility and above 3 cm/s for locomotion for more than 90% of the time). In total, we analyzed 511 cell pairs from 5 sessions. Indeed, the cross-correlation of subVm between cell pairs revealed a

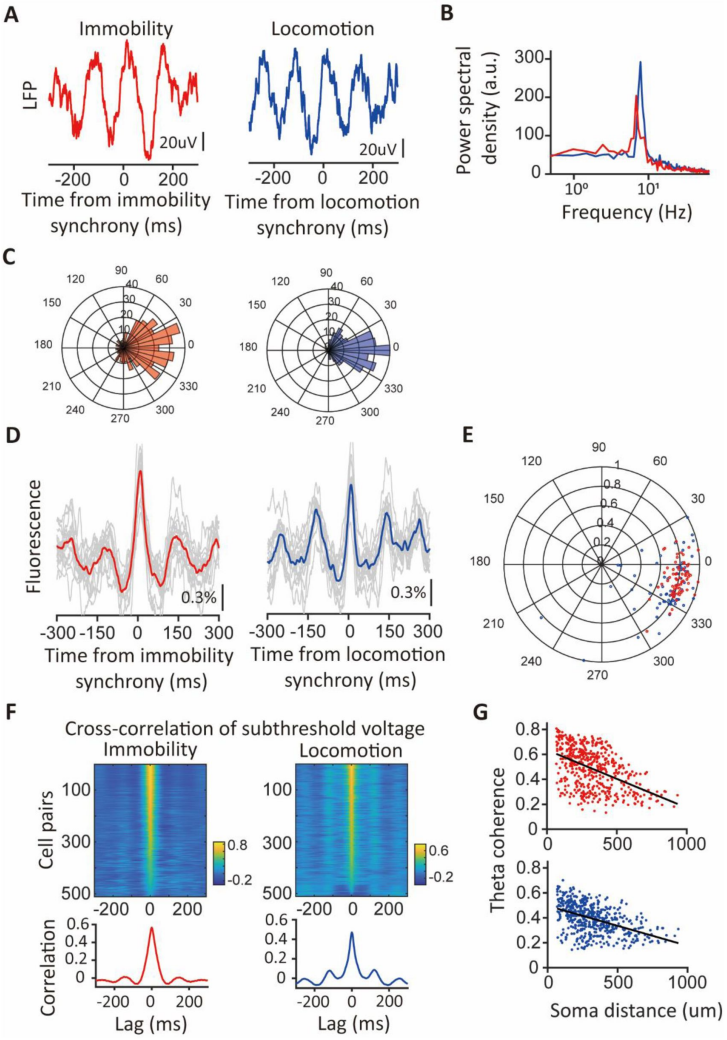

Figure 4

Theta oscillations in the LFP and subthreshold membrane potential were linked to population synchrony.

(A) LFP waveforms triggered by timings of synchronous ensembles. Red: triggered by timings of immobility synchrony; blue: triggered by timings of locomotion synchrony.
(B) Power spectral densities of the triggered LFP waveforms. Red: immobility; blue: locomotion.
(C) Distributions of the differences between LFP theta phases of individual synchronous ensembles and their preferred phases of the session. Note that most ensembles show minor differences within ±30 degrees. Red: immobility; blue: locomotion.
(D) Fluorescence traces triggered by timings of synchronous ensembles. Traces with spikes are excluded. Left panel: traces triggered by timings of immobility synchrony. Right panel: traces triggered by timings of locomotion synchrony. Thin gray lines: mean triggered fluorescence traces averaged across triggers for representative cells. Thick red and blue lines: mean triggered fluorescence traces averaged across cells.
(E) Polar plot illustrating theta modulation of spikes participating in the immobility synchrony (red dots) and of spikes participating in the locomotion synchrony (blue dots). The angle of the dots indicates the preferred phase, and the distance from the center of the circle represents the modulation strength. Each dot represents the averages from a neuron.
(F) Pairwise cross-correlation of the subthreshold membrane voltages (subVm). Top: color-coded cross-correlation of subVm between cell pairs during immobility and locomotion periods. Bottom: averaged cross-correlation over all cell pairs for immobility (red) and locomotion (blue) subVm. Both show a central peak at zero lag flanked by theta oscillation.
(G) Scatter plots of theta coherence against soma distances of immobility subVm (red) and locomotion subVm (blue) between cell pairs.

high correlation at zero lag and periodic modulation of the correlation at theta frequency (**Figure 4F**). Furthermore, the subVm theta coherences were increased in both groups (immobility: 0.50, locomotion: 0.40, median, n=511 pairs) and were negatively correlated with soma distances (immobility:-0.46, locomotion:-0.48, n=511 pairs, **Figure 4G**). Taken together, during novel exploration, CA1PCs generate synchronous activity associated with theta oscillation and exhibit correlated and theta-coherent subVms.

Synchrony between place cells with distinct place tunings

When animals explore a novel maze, spatially tuned spiking activity can form within a few minutes[32,33]. However, how synchronous ensembles organize their spatially tuned activities during novel exploration remains to be determined. Synchronous ensembles, generating spikes coincidently in short intervals, might display correlated spiking at longer time windows that match behavioral timescales of exploration, potentially leading to shared place responses. On the other hand, CA1PCs are interconnected through inhibitory interneurons[34–36]. Modulation of activities in inhibitory interneurons by some place cells may influence the activities of other place cells, resulting in divergent spatial tunings[32,37,38].

To compare the spatial tunings of synchronous cell pairs, we first calculated the spatial tuning curves of individual neurons by computing the mean firing rates in every spatial bin. On average, 40% of cells displayed selective spatial tunings of their spiking activities and were qualified as place cells[39] (**Figure 5A**). Among place cell pairs, some showed similar spatial tunings, while others did not (**Figure 5B**). For instance, in an illustrative session depicted in **Figure 5B**, the seventh and eighth place cells had highly similar spatial tunings with a correlation coefficient as high as 0.7. In contrast, the fifth and tenth place cells exhibited vastly different spatial tunings with a correlation coefficient as low as-0.5.

We further explored the relationship between the similarity of spatial tunings and synchronization strength among pairs of place cells. We measured synchronization strength as the peak of the CCG normalized by the averaged jittered spike count within the same bin as the CCG peak. We segregated spikes based on these behavioral states to accommodate differences between locomotion and immobility and calculated the corresponding CCG and synchronization strength.

During locomotion, we observed a robust negative correlation between synchronization strength and the similarity of spatial tunings among cell pairs. In other words, cell pairs with more precisely co-active spikes during locomotion exhibited more distinct place-tuning profiles (**Figure 5C** and **5D**). This anti-correlation between synchronization strength and place tunings indicates coordination between place cells' temporal and spatial coding. On the other hand, synchronization strength during immobility showed little correlation with the similarity of spatial tunings among place cell pairs, suggesting that correlated activities at the millisecond timescale do not extend to slow, behavioral-relevant timescales (**Figure 5**-figure supplement 1). Thus, place cells with distinct place fields are linked by synchronous activity during novel locomotion.

Discussion

Our findings reveal the presence of synchronous ensembles comprising a substantial number of CA1PCs during both locomotion and immobility in a novel environment. These ensembles concurrently engage neurons representing diverse aspects of the environment and are rarely observed during ripple events. Instead, they closely align with LFP and intracellular theta oscillations. Our data demonstrate theta-associated synchronous ensembles during spatial memory acquisition, coordinating numerous CA1 place cells that transmit information about different segments of the environment.

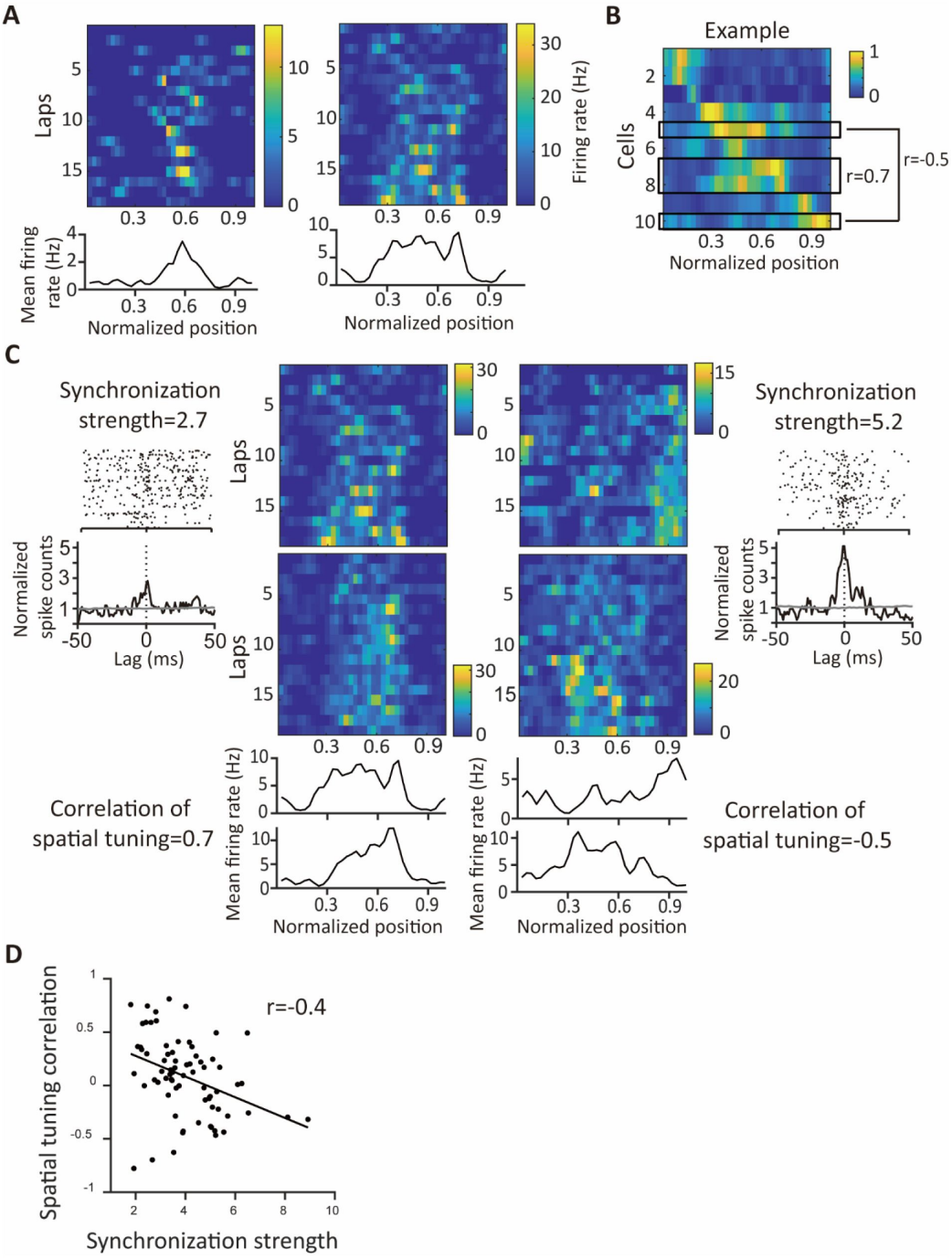

Figure 5

Negative correlation between spatial tuning similarity and synchronization strength during novel exploration.

(A) Spatially binned rate maps of place cells. High firing rates are indicated in yellow, and low firing rates are noted in blue. Bottom: the mean firing rates along spatial bins averaged across laps.
(B) Spatial tunings of 10 place cells from an example session. Cells are sorted based on the locations of their peak firing rates.
(C) Two example pairs of neurons with cross correlograms during locomotion and spatially binned firing rate maps.
(D) A scatter plot of correlation coefficients of spatial tunings against synchronization strengths for place cell pairs. Each dot represents a pair of place cells. Synchronization strengths are negatively correlated with similarities of spatial tunings (Spearman correlation coefficient=-0.4, $p<0.001$, $n=73$ pairs).

The correlation between observed population synchrony and theta oscillations is intriguing. Theta oscillations are typically associated with the sequential activation of neurons over time, resulting in reduced neuronal synchrony[22]. However, theta oscillations come in different types, each characterized by distinct pharmacological properties and behavioral correlates[40–42]. For example, type 1 theta, referred to as translational theta, occurs during voluntary movements and is sensitive to N-methyl-D-aspartate receptor (NMDAR) blockers. On the other hand, type 2 theta, known as attentional theta, is blocked by muscarinic receptor antagonists, emerging during states of arousal or attention, such as entering a new environment[43–45].

During theta oscillations, cholinergic neurons in the medial septum excite downstream CA1PCs, leading to increased firing rates and membrane potentials[46–48]. Given the widespread influence of cholinergic inputs on numerous CA1PCs, theta-coupled cholinergic inputs may drive depolarization and firing across many CA1PCs. Additionally, they could enhance the likelihood of synchronicity. Furthermore, GABAergic neurons in the medial septum, activated during theta oscillations, could activate interneurons in the CA1 region[42,49,50]. These CA1 interneurons, in turn, have the capability to entrain the activities of pyramidal neurons at both sub-and suprathreshold levels, thereby promoting synchronization among pyramidal neurons[51,52]. In summary, cholinergic and GABAergic neuron activation during theta waves may contribute to the excitation of CA1PCs and the consequent increase in their synchronicity.

Theta oscillations have long been implicated in memory acquisition. Specifically, theta power correlates positively with learning performance[53–55]. Perturbing generation of theta waves leads to impairment in memory acquisition[56–60], while electrical stimulation restoring theta rhythms rescues learning performance[61,62]. Furthermore, increased spike-theta coherence correlates with better memory, and stimulations that boost theta phase-locking of spikes enhance memory[63–65]. Despite abundant evidence supporting a link between theta oscillations and memory, the precise network mechanism by which theta oscillations support memory acquisition remains unclear. Theta oscillations are hypothesized to link spatially distributed neurons into functional ensembles to support memory acquisition[13]. The identified synchronous ensembles support the hypothesis, providing a network substrate that links theta rhythms to the initial stage of memory acquisition.

Previous reports of CA1 synchronous ensembles occur predominantly during ripple oscillations[8,14,17]. However, we found only a few ripple events in the initial minutes of entering a new environment, even when animals are not moving. During these events, CA1PCs show decreased spiking activities, and they display synchronous firing outside ripple episodes (**Fig.3**). Different from the ripple-associated synchronous ensembles described previously, the synchronous ensembles we observed involve larger populations of neurons spiking synchronously in narrower time intervals and are associated with theta oscillations. The absence of recorded ripple-associated synchrony in our study may be attributed to elevated arousal with prominent theta oscillations even during immobility, potentially suppressing ripples[66]. Additionally, the deep-layer CA1PCs imaged in our study are known to show decreased activities during ripples, contributing to their lack of ripple-associated synchrony[67]. The CA1 network may generate multiple types of population synchrony, with ripple-associated synchrony facilitating memory consolidation, while the newly identified theta population synchrony supports the initial stage of memory acquisition.

Although CA1PCs are known to exhibit weaker recurrent connectivity than that of CA3 pyramidal neurons, CA1PCs did communicate through monosynaptic connections[68]. These connections can be dynamically adjusted by the spike-timing-dependent plasticity mechanism[69–71], and therefore could be affected by the transient population synchrony. In addition, CA1PCs are known to communicate through inhibitory interneurons. Multiple pyramidal neurons converge onto a single interneuron, and individual connections are often weak and unreliable[35,72,73]. This connectivity scheme requires multiple pyramidal neurons spiking synchronously within the time

window of synaptic integration to effectively activate postsynaptic neurons[35]. Furthermore, population synchrony among CA1PCs may propagate to downstream areas, synchronizing neurons outside the hippocampus. With their large ensemble sizes, these synchronous ensembles may synergistically convey relevant information or reorganize the connectivity of the neuronal networks.

Prior studies in sensory systems have commonly revealed that neurons with synchronous activities typically share similar sensory responses[74,75]. However, the synchronous ensembles we have identified often encompass neurons with distinct preferences for place fields. Pairwise synchrony demonstrates a negative correlation with place field overlap (**Fig. 5**). These findings indicate that synchrony does not necessarily imply similar tunings between neurons. Furthermore, these synchronous ensembles involve place cells encoding different spatial information. Recognizing the crucial role of neuronal synchrony in binding distributed neurons in the brain[3,5], population synchrony may serve as a mechanism to integrate diverse features of the same environment into a cohesive mental map.

Methods

Animal

Time-pregnant wild-type C57BL/6J female mice underwent in utero virus injection of CamkII-cre virus (105558-AAV1, Addgene) into the left side of the lateral ventricles. The resulting offspring were raised in a breeding room under controlled temperature and humidity conditions and a 12-hour light/dark cycle (lights on from 7:00 to 19:00). The mice used in the experiments were between 12 and 18 weeks old at the time of the recordings. All surgical procedures, behavioral training, and recording protocols were approved by the NYCU Institutional Animal Care and Use Committee.

In-utero virus injection

Time-pregnant mice on an embryonic day 14.5 were anesthetized with isoflurane (induction:4-5%; maintenance:1-3%) before surgery. The animals were placed on a heating pad in a supine position to maintain body temperature. Aseptic procedures were implemented to maintain sterile conditions during the surgery. Uterine horns were exposed one at a time using spoons and fingers. Warm and sterile phosphate-buffered saline (PBS) was used to rinse the uterus to prevent it from drying out. Micropipettes loaded with CamkII-cre virus solution were used to inject 0.2 uL of virus suspension into the left side of the lateral ventricle of each embryo. The uterine horn was then gently returned to the abdominal cavity. The exact process was repeated to the other uterine horn. After the surgery, ketorolac (6mg/kg) and cefazolin (1g/kg) were administered for two days to minimize pain and inflammation.

Cranial window and cannula implantation

The offspring of the mice that had undergone in-utero injection were subjected to chronic hippocampal window surgery when they were between 2 and 4 months old. The animals were initially anesthetized using isoflurane (induction:4-5%; maintenance:1-3%). Topical anesthesia was applied by administering 0.5% lidocaine to the wound margins. After achieving deep anesthesia, an incision was made in the skin, and a circular section of the skull was removed, centered 2 mm caudal and 1.8 mm left to the bregma. Using 30-gauge needles and forceps, the dura was removed from the exposed area, and cortical tissue within the craniotomy was aspirated. A fine injection pipette (tip diameter 10-60 um) was used to inject AAV2/1-CAG-flex-Voltron2-ST (2.7×10^{12} GC/ml, a courtesy gift from Dr. Eric Schreiter and the GENIE team at HHMI Janelia Research Campus) into the exposed regions at a depth of 200 ìm (up to six injection sites and 100-200 nL of viral suspension). An optical chamber was constructed by placing a cannula with a cover slip attached

at the bottom over the craniotomy and sealing it with dental acrylic or C&B Metabond (Sun Medical). A custom-built titanium frame was then cemented to the animal's head using dental acrylic or C&B Metabond. Mice received ketorolac (6mg/kg) and cefazolin (1g/kg) for two days following surgery to minimize pain and inflammation.

Behavioral training

After at least two weeks of recovery from the window surgery, the mice underwent behavioral training to ensure they were calm and attentive in the test environment. The initial training phase involved acclimating the mice to head fixation and treadmill running, which took place over 3-5 days in a separate room distinct from the recording setup. Following this training, the imaging experiments were conducted. On the day designated for imaging, the mice were introduced to the recording room for the first time just before the imaging session. During the imaging experiments, the mice were securely held in a head-fixed position beneath the microscope and on an air-lifted plastic track that rested on an air table (AirLift, Neurotar; **Fig. 1Aa**). The track was adorned with various shapes of signs to help the mice navigate the track. Subdued blue lighting was provided to illuminate the track. Before the initiation of imaging, the mice were confined in a corner of the track using gates. Subsequently, the gates were opened upon the start of imaging, allowing the mice to explore the new environment during their initial laps (**Fig. 1Ab**). The Mobile HomeCage tracking system (Neurotar) was used to track the mice's position and speed. During the acquisition of image frames, TTL pulses were sent by the high-speed camera to the Mobile HomeCage tracking system to facilitate data alignment.

Voltage imaging

Imaging was performed after treadmill training. JF_{552}-HaloTag ligand[76] (a courtesy gift from Dr. Luke Lavis) was first dissolved in DMSO (Sigma) and then diluted in Pluronic^{TM} F-127 (P3000MP, Invitrogen) and PBS to achieve a final concentration of 0.83 mM of JF_{552}-HaloTag ligand. The solution was then injected intravenously through the retro-orbital sinus. Imaging sessions were initiated 3-5 hours after the injection of the JF_{552}-HaloTag ligand. Fluorescence sensors were excited using a 532-nm laser (Opus 532, Laser Quantum) with an excitation filter (FF02-520-28, Semrock), and the emitted light was separated from the excitation light using a dichroic mirror (540lpxr Chroma) and passed through an emission filter (FF01-596183 Semrock). A 16X, 0.8 NA objective (Nikon) was used to collect the emission light which was then imaged on a CMOS camera (DaVinci-1K, RedShirt) with a 50-mm camera lens (Nikkor 50mm f1.2, Nikon) as the tube lens. Images were acquired using Turbo-SM64 (Sci-Measure) at 2kHz with a resolution of 190 x 160 pixels, corresponding to a field of view of 1.4 x 1.2 mm. The number of frames in an image session was set at 360,000, corresponding to a duration of 180 seconds per session. Imaging depths ranged between 70 and 170 ìm from the window surface, where the CA1 pyramidal neurons were located. Time-lapse images were collected, and image stacks of the same field of view along the z-axis were acquired. The image stacks consisted of 100 plans separated by two ìm, covering the depth from the window surface to 200 um from the surface.

LFP recording

The LFP signal from the contralateral CA1 region of the hippocampus was simultaneously recorded during voltage imaging. To implant the LFP electrode, a small craniotomy was performed at the dorsal CA1 coordinate (2mm caudal and 1.8 mm right to the bregma). A tungsten electrode (#100211, 38 ìm in diameter, polyimide insulated, California Fine Wire) was inserted into the dorsal CA1 region, and the wire and pins were cemented in place with dental acrylic. The electrical signal was amplified and filtered (1-1kHz) using a DAM80 amplifier (Word Precision Instruments). The amplified signal was acquired by an I/O device (National Instruments USB-6341) and recorded using WaveSurfer (Adam Taylor, HHMI Janelia Research Campus) at 10 kHz during implantation and TurboSM64 (RedShirt) at 8 kHz during imaging.

Voltage imaging preprocessing and spike detection

Fluorescence intensities were corrected for brain movement using rigid registration. Regions of interest (ROIs) were manually selected by grouping pixels that cover individual somata. The fluorescence intensities of individual neurons were calculated by averaging the fluorescence intensities of pixels from the same ROIs. Bleaching was corrected by calculating the baseline fluorescence (F_0) at each time point as an average of the fluorescence intensities within ±0.5 s around the time point. The dF/F was calculated as the F_0 minus the fluorescence intensity of the same time point divided by F_0. Positive fluorescence transients were detected to identify spikes from the high-passed dF/F traces created by subtracting the dF/F traces from the median-filtered version with a 5-ms window. To simulate the noise of recordings, high-passed dF/F traces were inverted, and the amplitudes of the transients detected from the inverted traces were used to construct a noise distribution of the spike amplitudes. A threshold was set by comparing the amplitudes of the detected transients with the noise distribution of the spike amplitudes to minimize the sum of type I and type II errors. Spikes were first detected when transients were larger than the threshold. Then, spike amplitudes smaller than half of the top 5% spike amplitudes were excluded. The signal-to-noise ratio (SNR) was calculated for each neuron as a ratio of the averaged spike amplitudes over the standard deviation of the high-passed dF/F traces, excluding points 2 ms before and 4 ms after each detected spike to estimate the quality of the recordings. The crosstalk between ROIs was routinely checked by examining the refractory periods of neurons in auto-correlograms. Only neurons meeting the following criteria were included: (1) SNR larger than 5, (2) full width at half maximum of the spike waveform longer than 0.8 ms, (3) mean spike rates higher than 0.1 Hz, (4) distances between soma pairs at least 70 ìm. Sessions with at least nine neurons meeting the selection criteria were used for further analysis. Based on these criteria, we included five sessions containing 9, 11, 13, 19, and 19 neurons.

Behavioral states of locomotion and immobility

The periods of locomotion were defined as instances when the animals' speed exceeded 3 cm/s, while periods of immobility were determined as instances when the animals' speed fell below 1 cm/s.

Mean firing rates during locomotion and immobility

To calculate the mean firing rates during locomotion, we counted the number of spikes during locomotion periods and divided this number by the total duration of locomotion. Similarly, for mean firing rates during immobility, we calculated the number of spikes that occurred during immobility periods and divided this number by the total duration of immobility.

Correlation between instantaneous firing rate and animal speed

To estimate the instantaneous firing rates of individual neurons over time, we convolved their spike trains with a Gaussian window of 250 ms. Subsequently, we calculated the Pearson correlation coefficient between these instantaneous firing rates and the animal's speed for each neuron.

Grand average cross-correlogram (CCG)

Grand average CCGs were generated by constructing histograms of relative spike timings between spikes of a reference cell and spikes of all other neurons in the same session as the target cell population. Histograms were binned using 1-ms time bins. Spike counts were normalized by the number of reference spikes times the number of all other neurons. An equal number of cells from different sessions were randomly selected to form the shuffled target cell population to assess the statistical significance of the CCG peaks. Subsequently, grand average CCGs were computed using

shuffled spike trains for comparison. Grand average CCGs were calculated using all spikes in the 180-s recording periods, subsets of spikes during immobility periods (immobility grand average CCGs), and subsets of spikes during locomotion periods (locomotion grand average CCGs).

Detection of the population synchrony

To assess population synchrony, we counted the number of spikes from all neurons within a sliding window of 25 ms. To test the significance of the synchrony, we generated surrogate data by jittering spike timings within a ±75-ms window. By comparing the spike counts between the original and jittered populations, we determined population synchrony when the spike count was higher than the mean plus four standard deviations of the jittered spike counts. To estimate synchronous event rates, we divided the entire 180-s recordings into halves and calculated the event rate in each of the 90-s segments. Additionally, we quantified the ensemble sizes by counting the percentage of participating neurons in each synchronous event.

Pairwise cross-correlogram (CCG) of neuronal pairs

To compute the CCG, we first determined the time difference between spikes in the target and reference neurons and then binned these values into 1-ms time bins. CCGs were only computed for pairs with more than 100 counts within the CCG window of ±500 ms to ensure reliable correlation. We defined the peak of the CCG as the local maxima within ±30 ms of lag. To assess the significance of cross-correlations, we generated surrogate data by jittering the spike times of the target neuron within a ±75 ms window. We computed the CCG peak for a thousand iterations and calculated p-values by comparing the percentile of the peak in the null distribution of the jittered peak values. The synchronization strength was estimated as the ratio between the original CCG peak and the mean spike count of the same bin as the original CCG peak averaged across the jittered histograms. For display purposes, the CCGs were smoothed using a 5-point moving average. CCGs were calculated using all spikes in the 180-s recording periods, subsets of spikes during immobility periods (immobility pairwise CCGs), and subsets of spikes during locomotion periods (locomotion pairwise CCGs).

LFP ripple analysis

To detect ripples, we performed band-pass filtering of the LFP signal between 120 and 240 Hz, followed by computing the envelope using the absolute values of the Hilbert transform, which was then low-pass filtered at 20 Hz. The start and end times of ripples were identified by setting the upper and lower thresholds at the mean plus 7 and 3.5 times the standard deviation of the envelope, respectively. For a ripple event to be included, three conditions had to be met: (1) values within the event were higher than the lower threshold, (2) at least one value exceeded the upper threshold, and (3) the minimum duration of the event was 30 ms. The start and end times of a ripple event were defined as the positive and negative crossings of the lower threshold, respectively. We defined in-ripple periods as the time between the start and end of detected LFP ripple events, while out-ripple periods were periods outside the in-ripple periods. The envelope peak values of the detected ripple events were used as the time of ripple occurrence. These timings were utilized as trigger timings to calculate averages triggered by ripples. Two co-occurrences were quantified: the percentages of LFP ripple oscillations that occurred with synchronous ensembles and the percentages of synchronous ensembles that occurred with LFP ripple oscillations.

Ripple modulation index

We utilized the ripple modulation index to assess changes in firing rates during ripples compared to periods outside ripples. This index was computed as the ratio of the difference in mean firing rates during in-and out-ripple periods to the sum of the mean firing rates during both periods. Specifically, we first calculated the mean firing rate during in-ripple periods and the mean firing rate during out-ripple periods. Next, we subtracted the mean firing rate during out-ripple periods

from the mean firing rate during in-ripple periods and divided the result by the sum of the mean firing rates during both periods. The resulting ripple modulation index indicates the magnitude and direction of the firing rate modulation during ripple compared to periods outside ripples.

LFP traces triggered by population synchrony and analysis

The midpoints of the synchronous event intervals were utilized as triggers to align LFP traces. These traces were aligned within a ±1-second window around the trigger time points. To calculate the spectral density functions of the aligned LFP traces, we performed a 16,384-point fast Fourier transform of the 2-second LFP traces. The power spectra were then estimated as the squared absolute values of the Fourier coefficients. Ripple power was calculated as the sum of the power distributed between 120 and 240 Hz. To calculate theta modulation strength and preferred angles of the synchronous ensembles, LFP was first filtered within the theta frequency range. Then, the phase $\phi(t)$ and the instantaneous amplitude $A(t)$ of the filtered LFP were computed using the Hilbert transform. A vector $V_k = A(t_k)e^{i\phi(tk)}$ was assigned to each synchronous ensemble that occurred at time t_k. The modulation strength and the preferred phase angle were determined as the absolute value and the phase angle of the summed vector over all ensembles, respectively. Modulation strengths were normalized by the total length of all vectors.

Subthreshold membrane voltage (subVm)

To compute the subVm of individual neurons, we began by determining the difference between the raw dF/F signal and the high-pass version of dF/F. Next, we calculated the spike threshold for each cell by identifying the voltage value corresponding to the peak of the first derivative of the spike waveforms. Any fluorescence values in the slow dF/F time courses that surpassed the spike thresholds were linearly interpolated.

SubVm traces triggered by population synchrony

The midpoint of the time intervals, during which synchronous ensembles were detected, served as the reference points for aligning fluorescence traces within a ±300 ms window around those reference points. To eliminate any interference from membrane potential fluctuations associated with spikes, we excluded aligned traces in cases where any spike occurred within the time intervals of the aligned traces.

SubVm theta modulation and phase preference of spikes occurred inside and outside the population synchrony events

The subVm was initially filtered within the theta frequency range. Subsequently, the phase $\phi(t)$ and the instantaneous amplitude $A(t)$ of the filtered subVm were computed using the Hilbert transform. Spikes were categorized into four groups: those occurring during or outside immobility synchronous events and those occurring during or outside locomotion synchronous events. Within each category, a vector $V_k = A(t_k)e^{i\phi(tk)}$ was assigned to each spike that occurred at time t_k. The modulation strength and the preferred phase angle were determined as the absolute value and the phase angle of the summed vector over all spikes, respectively. Modulation strengths were normalized by the total length of all vectors to facilitate comparison between neurons.

Spike-triggered fluorescence traces

We extracted segments of fluorescence traces using a ±300 ms time window centered on the spike timings. To examine variations in fluorescence waveforms triggered by spikes within and outside synchronous events, we categorized the fluorescence traces based on whether the spikes occurred within or outside these events. Subsequently, we performed pairwise comparisons of the fluorescence values from the same neuron, concentrating on spikes occurring during corresponding behavioral states. Neurons with fewer than four triggering events in any of these categories were omitted from the analysis.

Cross-correlation and coherence analysis to the subVm traces

To calculate cross-correlation and theta coherence of subVm between pairs of neurons during locomotion and immobility, we initially divided the 180-second subVm traces into 1-second segments with a 50% overlap. These segments were then categorized into the locomotion group if the animal's speed remained above three cm/s for more than 90% of the time within that segment. Similarly, segments were sorted into the immobility group if the animal's speed remained below one cm/s for more than 90% of the time within that segment. Subsequently, we computed the cross-correlation and magnitude-squared coherence function of frequency for pairs of co-occurred segments belonging to a specific cell pair. Mean cross-correlations of individual cell pairs were averaged across segments that occurred in the same behavioral states (i.e., locomotion or immobility states). To estimate theta coherence, we averaged the values of the coherence function within the theta frequency range (4-12 Hz). Theta coherences from the same cell pair during the same behavioral state were pooled together, and the average was used as an estimate for the theta coherence of that cell pair during a particular behavioral state. Finally, Spearman correlation coefficients were calculated between the mean theta coherences of cell pairs and their soma distances.

Spatial analysis

We partitioned a 90-cm-long track into 36 spatial bins to analyze spatial tuning properties. For each cell, the spatial tuning curve was computed by determining the mean firing rate, defined as the number of spikes within the bin when the animal's speed exceeded three cm/s, divided by the total dwell times using the same speed threshold. The peak firing rates were identified as the maximal rate on the spatial tuning curve. Spatial selectivity was calculated as one minus the circular variance of the spatial tuning curve. Neurons were classified as place cells when their spatial selectivity exceeded 0.25, and peak firing rates exceeded 1 Hz. To assess the similarity of spatial tuning between pairs of neurons, Spearman correlation coefficients were calculated for the spatial tuning curves. To explore the relationship between levels of synchronization and spatial tuning similarity among pairs of place cells, Spearman correlation coefficients were computed between synchronization strengths of cell pairs and correlation coefficients of their spatial tuning curves.

Data analysis and statistics

Data analysis was performed using MATLAB (Mathworks, R2019b), and results were presented as standard error of the mean unless otherwise specified. Boxplots were used to depict the median, first quartile, and third quartile, with the middle line, the upper edge, and the lower edge of the box, respectively. The whiskers of the boxplots represented the 5th and 95th percentiles of the distribution.

Acknowledgements

We express our sincere gratitude to Dr. Luke Lavis for sharing the JF_{552}-HaloTag ligand. Special thanks to Mr. Yu-Ting Lin and Ms. Hui-Ching Chen for technical assistance. We are grateful to Drs. Shih-Chieh Lin, Kuo-Hua Huang, Shi-Bing Yang, and Fu-Chin Liu for their insightful comments on the manuscript.

Funding statements

National Science and Technology Council, Taiwan (B.-J.L. and T.-W.C.) Howard Hughes Medical Institute, USA (E.R.S.)

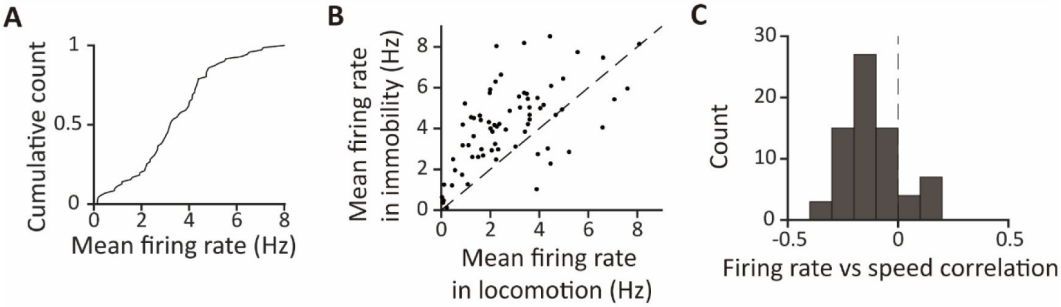

Supplementary Figure 1

Mean firing rate distribution and correlation with animals' speed.

(A) Cumulative distribution of mean firing rates averaged throughout the entire 180-second recording period.
(B) Mean firing rates during locomotion plotted against mean firing rates during immobility for individual cells. Each dot represents a cell. Mean firing rates are higher during immobility than during locomotion (4.2±0.2 Hz for immobility, 2.8±0.2 Hz for locomotion, n=71 cells, p<0.001, Wilcoxon signed-rank test).
(C) Histogram of correlation coefficients between instantaneous firing rates and the animals' speed for each neuron.

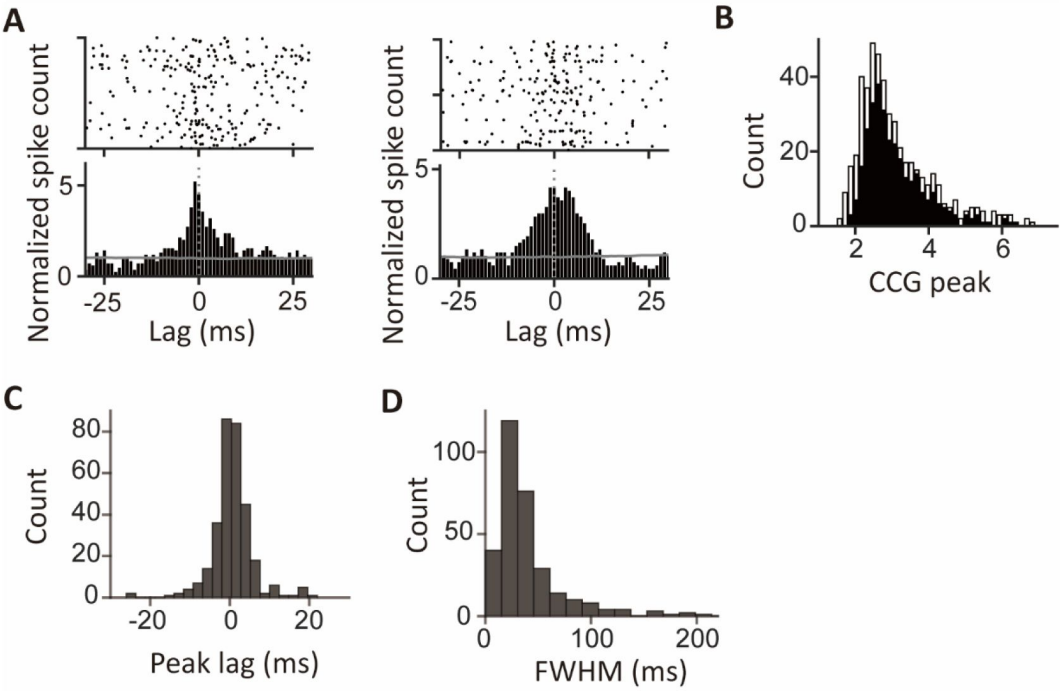

Figure 1-figure supplement 1

Pairwise cross-correlogram (CCG) between CA1 pyramidal cells.

(A) CCGs of two representative cell pairs exhibiting significant peaks compared to the jittered spike trains of the target cells (gray lines).
(B) Distribution of the CCG peaks (n=497 pairs). Black: CCG peaks with significance (p<0.05). White: CCG peaks without significance (p>=0.05).
(C) Histogram of peak lags of significant CCG peaks (n=315 pairs).
(D) Histogram of FWHMs of significant CCG peaks (n=315 pairs).

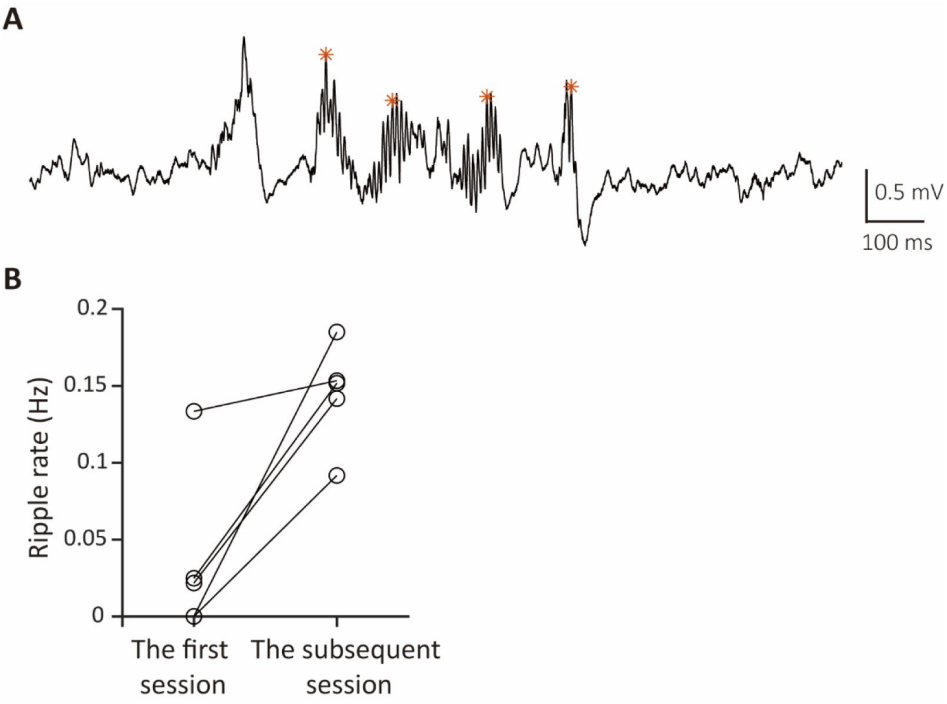

Figure 3-figure supplement 1

LFP ripples recorded in the first and subsequent sessions in a novel maze.

(A) An example LFP trace with ripples recorded in a subsequent session following the first session of novel exploration, where no ripple was detected.
(B) Ripple rates in the first and subsequent sessions recorded in the same animals (n=5 mice) during novel exploration.

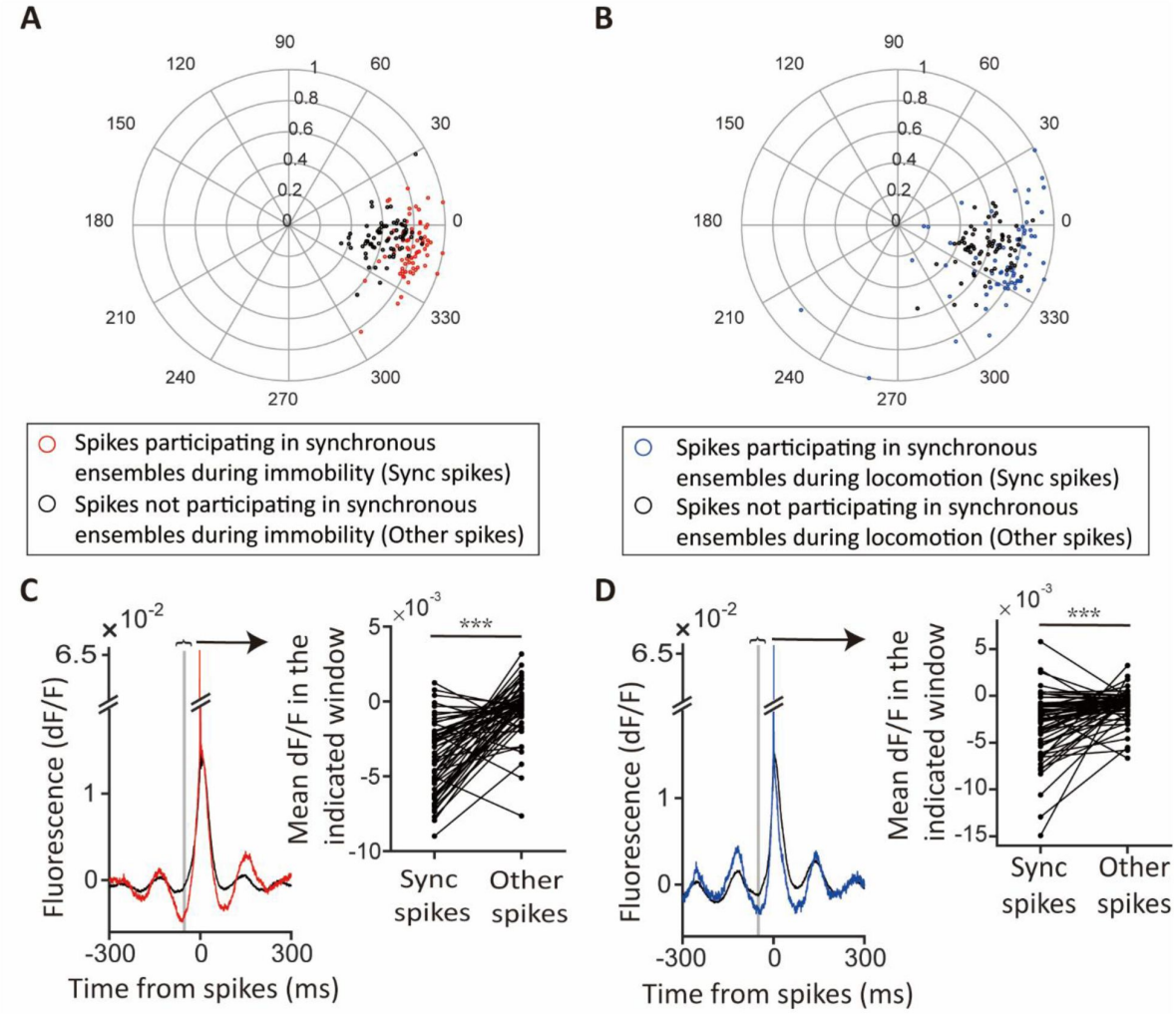

Figure 4-figure supplement 1

Theta modulation of spikes during immobility and locomotion periods of novel exploration.

(A) Polar plot comparing theta modulation between spikes participating in synchronous ensembles (sync spikes) and spikes not participating in synchronous ensembles (other spikes) during immobility. Each dot represents the averaged modulation of a cell. The modulation strengths of spikes participating in synchrony are significantly higher than those of spikes not participating in synchrony (modulation strength for spikes participating in synchronous ensembles: 0.81±0.08, for spikes not participating in synchronous ensembles: 0.63±0.12, mean±s.d., n=71 cells, p<0.001, pair Student's t-test).
(B) Same as in (A), but during locomotion (modulation strength for spikes participating in synchronous ensembles: 0.76±0.18, for spikes not participating in synchronous ensembles: 0.60± 0.12, mean±s.d., n=71 cells, p<0.001, pair Student's t-test).
(C) Average fluorescence triggered by cells' spikes participating in synchronous ensembles (red, sync spikes) and not participating in synchronous ensembles during immobility (black, other spikes; n=59 cells). Inset: Pairwise comparison of average fluorescence 50±5 ms before time of spikes (t=0) between the two triggered groups (n=59 cells).
(D) Same as in (C), but during locomotion.

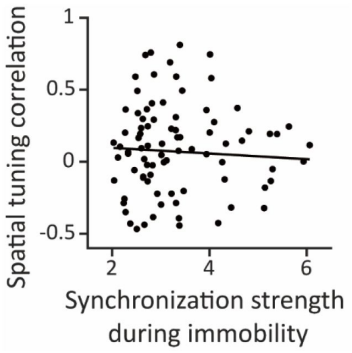

Figure 5-figure supplement 1

Synchronization strengths during immobility show little correlation with the similarity of spatial tunings between place cells.

Synchronization strengths during immobility plotted against correlation coefficients of spatial tunings for pairs of place cells. Synchronization strengths show little correlation with similarities of spatial tunings (Spearman correlation coefficient=-0.003, p=0.98, n=88 cell pairs).

References

1 Takeuchi T., Duszkiewicz A. J., Morris R. G (2014) **The synaptic plasticity and memory hypothesis: encoding, storage and persistence** *Philos Trans R Soc Lond B Biol Sci* **369** https://doi.org/10.1098/rstb.2013.0288

2 Moser M. B., Rowland D. C., Moser E. I (2015) **Place cells, grid cells, and memory** *Cold Spring Harb Perspect Biol* **7** https://doi.org/10.1101/cshperspect.a021808

3 Axmacher N., Mormann F., Fernandez G., Elger C. E., Fell J (2006) **Memory formation by neuronal synchronization** *Brain Res Rev* **52**:170–182 https://doi.org/10.1016/j.brainresrev.2006.01.007

4 Paulsen O., Sejnowski T. J (2000) **Natural patterns of activity and long-term synaptic plasticity** *Curr Opin Neurobiol* **10**:172–179 https://doi.org/10.1016/s0959-4388(00)00076-3

5 Wang X. J (2010) **Neurophysiological and computational principles of cortical rhythms in cognition** *Physiol Rev* **90**:1195–1268 https://doi.org/10.1152/physrev.00035.2008

6 Harris K. D., Csicsvari J., Hirase H., Dragoi G., Buzsaki G (2003) **Organization of cell assemblies in the hippocampus** *Nature* **424**:552–556 https://doi.org/10.1038/nature01834

7 Squire L. R., Wixted J. T (2011) **The cognitive neuroscience of human memory since H.M** *Annu Rev Neurosci* **34**:259–288 https://doi.org/10.1146/annurev-neuro-061010-113720

8 Buzsaki G (2015) **Hippocampal sharp wave-ripple: A cognitive biomarker for episodic memory and planning** *Hippocampus* **25**:1073–1188 https://doi.org/10.1002/hipo.22488

9 Nadasdy Z., Hirase H., Czurko A., Csicsvari J., Buzsaki G (1999) **Replay and time compression of recurring spike sequences in the hippocampus** *J Neurosci* **19**:9497–9507 https://doi.org/10.1523/JNEUROSCI.19-21-09497.1999

10 Cheng S., Frank L. M (2008) **New experiences enhance coordinated neural activity in the hippocampus** *Neuron* **57**:303–313 https://doi.org/10.1016/j.neuron.2007.11.035

11 Dragoi G., Tonegawa S (2011) **Preplay of future place cell sequences by hippocampal cellular assemblies** *Nature* **469**:397–401 https://doi.org/10.1038/nature09633

12 Liu C., Todorova R., Tang W., Oliva A., Fernandez-Ruiz A (2023) **Associative and predictive hippocampal codes support memory-guided behaviors** *Science* **382** https://doi.org/10.1126/science.adi8237

13 Colgin L. L (2016) **Rhythms of the hippocampal network** *Nat Rev Neurosci* **17**:239–249 https://doi.org/10.1038/nrn.2016.21

14 Buzsaki G., Silva F. L (2012) **High frequency oscillations in the intact brain** *Prog Neurobiol* **98**:241–249 https://doi.org/10.1016/j.pneurobio.2012.02.004

15 Csicsvari J., Hirase H., Czurko A., Buzsaki G (1998) **Reliability and state dependence of pyramidal cell-interneuron synapses in the hippocampus: an ensemble approach in the behaving rat** *Neuron* **21**:179–189 https://doi.org/10.1016/s0896-6273(00)80525-5

16 Gillespie A. K., et al. (2021) **Hippocampal replay reflects specific past experiences rather than a plan for subsequent choice** *Neuron* **109**:3149–3163 https://doi.org/10.1016/j.neuron.2021.07.029

17 Yagi S., Igata H., Ikegaya Y., Sasaki T (2023) **Awake hippocampal synchronous events are incorporated into offline neuronal reactivation** *Cell Rep* **42** https://doi.org/10.1016/j.celrep.2023.112871

18 El-Gaby M., et al. (2021) **An emergent neural coactivity code for dynamic memory** *Nat Neurosci* **24**:694–704 https://doi.org/10.1038/s41593-021-00820-w

19 Skaggs W. E., McNaughton B. L., Wilson M. A., Barnes C. A (1996) **Theta phase precession in hippocampal neuronal populations and the compression of temporal sequences** *Hippocampus* **6**:149–172 https://doi.org/10.1002/(SICI)1098-1063(1996)6:2<149::AID-HIPO6>3.0.CO;2-K

20 Dragoi G., Buzsaki G (2006) **Temporal encoding of place sequences by hippocampal cell assemblies** *Neuron* **50**:145–157 https://doi.org/10.1016/j.neuron.2006.02.023

21 Foster D. J., Wilson M. A (2007) **Hippocampal theta sequences** *Hippocampus* **17**:1093–1099 https://doi.org/10.1002/hipo.20345

22 Mizuseki K., Buzsaki G (2014) **Theta oscillations decrease spike synchrony in the hippocampus and entorhinal cortex** *Philos Trans R Soc Lond B Biol Sci* **369** https://doi.org/10.1098/rstb.2012.0530

23 O'Keefe J., Recce M. L (1993) **Phase relationship between hippocampal place units and the EEG theta rhythm** *Hippocampus* **3**:317–330 https://doi.org/10.1002/hipo.450030307

24 Lee A. K., Brecht M (2018) **Elucidating Neuronal Mechanisms Using Intracellular Recordings during Behavior** *Trends Neurosci* **41**:385–403 https://doi.org/10.1016/j.tins.2018.03.014

25 Petersen C. C. H (2017) **Whole-Cell Recording of Neuronal Membrane Potential during Behavior** *Neuron* **95**:1266–1281 https://doi.org/10.1016/j.neuron.2017.06.049

26 Giocomo L. M., Zilli E. A., Fransen E., Hasselmo M. E (2007) **Temporal frequency of subthreshold oscillations scales with entorhinal grid cell field spacing** *Science* **315**:1719–1722 https://doi.org/10.1126/science.1139207

27 Lampl I., Reichova I., Ferster D (1999) **Synchronous membrane potential fluctuations in neurons of the cat visual cortex** *Neuron* **22**:361–374 https://doi.org/10.1016/s0896-6273(00)81096-x

28 Poulet J. F., Petersen C. C (2008) **Internal brain state regulates membrane potential synchrony in barrel cortex of behaving mice** *Nature* **454**:881–885 https://doi.org/10.1038/nature07150

29 Abdelfattah A. S., et al. (2023) **Sensitivity optimization of a rhodopsin-based fluorescent voltage indicator** *Neuron* https://doi.org/10.1016/j.neuron.2023.03.009

30 Adam Y., et al. (2019) **Voltage imaging and optogenetics reveal behaviour-dependent changes in hippocampal dynamics** *Nature* **569**:413–417 https://doi.org/10.1038/s41586-019-1166-7

31 Klausberger T., et al. (2003) **Brain-state-and cell-type-specific firing of hippocampal interneurons in vivo** *Nature* **421**:844–848 https://doi.org/10.1038/nature01374

32 Rolotti S. V., et al. (2022) **Local feedback inhibition tightly controls rapid formation of hippocampal place fields** *Neuron* **110**:783–794 https://doi.org/10.1016/j.neuron.2021.12.003

33 Sheffield M. E. J., Adoff M. D., Dombeck D. A (2017) **Increased Prevalence of Calcium Transients across the Dendritic Arbor during Place Field Formation** *Neuron* **96**:490–504 https://doi.org/10.1016/j.neuron.2017.09.029

34 Takacs V. T., Klausberger T., Somogyi P., Freund T. F., Gulyas A. I (2012) **Extrinsic and local glutamatergic inputs of the rat hippocampal CA1 area differentially innervate pyramidal cells and interneurons** *Hippocampus* **22**:1379–1391 https://doi.org/10.1002/hipo.20974

35 English D. F., et al. (2017) **Pyramidal Cell-Interneuron Circuit Architecture and Dynamics in Hippocampal Networks** *Neuron* **96**:505–520 https://doi.org/10.1016/j.neuron.2017.09.033

36 Maccaferri G., Roberts J. D., Szucs P., Cottingham C. A., Somogyi P (2000) **Cell surface domain specific postsynaptic currents evoked by identified GABAergic neurones in rat hippocampus in vitro** *J Physiol* **524**:91–116 https://doi.org/10.1111/j.1469-7793.2000.t01-3-00091.x

37 Geiller T., et al. (2022) **Local circuit amplification of spatial selectivity in the hippocampus** *Nature* **601**:105–109 https://doi.org/10.1038/s41586-021-04169-9

38 Trouche S., et al. (2016) **Recoding a cocaine-place memory engram to a neutral engram in the hippocampus** *Nat Neurosci* **19**:564–567 https://doi.org/10.1038/nn.4250

39 Go M. A., et al. (2021) **Place Cells in Head-Fixed Mice Navigating a Floating Real-World Environment** *Front Cell Neurosci* **15** https://doi.org/10.3389/fncel.2021.618658

40 Kramis R., Vanderwolf C. H., Bland B. H (1975) **Two types of hippocampal rhythmical slow activity in both the rabbit and the rat: relations to behavior and effects of atropine, diethyl ether, urethane, and pentobarbital** *Exp Neurol* **49**:58–85 https://doi.org/10.1016/0014-4886(75)90195-8

41 Bland B. H (1986) **The physiology and pharmacology of hippocampal formation theta rhythms** *Prog Neurobiol* **26**:1–54 https://doi.org/10.1016/0301-0082(86)90019-5

42 Buzsaki G (2002) **Theta oscillations in the hippocampus** *Neuron* **33**:325–340 https://doi.org/10.1016/s0896-6273(02)00586-x

43 Sainsbury R. S., Heynen A., Montoya C. P (1987) **Behavioral correlates of hippocampal type 2 theta in the rat** *Physiol Behav* **39**:513–519 https://doi.org/10.1016/0031-9384(87)90382-9

44 Sainsbury R. S (1998) **Hippocampal theta: a sensory-inhibition theory of function** *Neurosci Biobehav Rev* **22**:237–241 https://doi.org/10.1016/s0149-7634(97)00011-0

45 Barry C., Heys J. G., Hasselmo M. E (2012) **Possible role of acetylcholine in regulating spatial novelty effects on theta rhythm and grid cells** *Front Neural Circuits* **6** https://doi.org/10.3389/fncir.2012.00005

46 Nakajima Y., Nakajima S., Leonard R. J., Yamaguchi K (1986) **Acetylcholine raises excitability by inhibiting the fast transient potassium current in cultured hippocampal neurons** *Proc Natl Acad Sci U S A* **83**:3022–3026 https://doi.org/10.1073/pnas.83.9.3022

47 Markram H., Segal M (1990) **Acetylcholine potentiates responses to N-methyl-D-aspartate in the rat hippocampus** *Neurosci Lett* **113**:62–65 https://doi.org/10.1016/0304-3940(90)90495-u

48 Fraser D. D., MacVicar B. A (1996) **Cholinergic-dependent plateau potential in hippocampal CA1 pyramidal neurons** *J Neurosci* **16**:4113–4128 https://doi.org/10.1523/JNEUROSCI.16-13-04113.1996

49 Toth K., Freund T. F., Miles R (1997) **Disinhibition of rat hippocampal pyramidal cells by GABAergic afferents from the septum** *J Physiol* **500**:463–474 https://doi.org/10.1113/jphysiol.1997.sp022033

50 Colgin L. L (2013) **Mechanisms and functions of theta rhythms** *Annu Rev Neurosci* **36**:295–312 https://doi.org/10.1146/annurev-neuro-062012-170330

51 Cobb S. R., Buhl E. H., Halasy K., Paulsen O., Somogyi P (1995) **Synchronization of neuronal activity in hippocampus by individual GABAergic interneurons** *Nature* **378**:75–78 https://doi.org/10.1038/378075a0

52 Stark E., et al. (2013) **Inhibition-induced theta resonance in cortical circuits** *Neuron* **80**:1263–1276 https://doi.org/10.1016/j.neuron.2013.09.033

53 Landfield P. W., McGaugh J. L., Tusa R. J (1972) **Theta rhythm: a temporal correlate of memory storage processes in the rat** *Science* **175**:87–89 https://doi.org/10.1126/science.175.4017.87

54 Berry S. D., Thompson R. F (1978) **Prediction of learning rate from the hippocampal electroencephalogram** *Science* **200**:1298–1300 https://doi.org/10.1126/science.663612

55 Belchior H., Lopes-Dos-Santos V., Tort A. B., Ribeiro S (2014) **Increase in hippocampal theta oscillations during spatial decision making** *Hippocampus* **24**:693–702 https://doi.org/10.1002/hipo.22260

56 Winson J (1978) **Loss of hippocampal theta rhythm results in spatial memory deficit in the rat** *Science* **201**:160–163 https://doi.org/10.1126/science.663646

57 Mitchell S. J., Rawlins J. N., Steward O., Olton D. S (1982) **Medial septal area lesions disrupt theta rhythm and cholinergic staining in medial entorhinal cortex and produce impaired radial arm maze behavior in rats** *J Neurosci* **2**:292–302 https://doi.org/10.1523/JNEUROSCI.02-03-00292.1982

58 Mizumori S. J., Perez G. M., Alvarado M. C., Barnes C. A., McNaughton B. L (1990) **Reversible inactivation of the medial septum differentially affects two forms of learning in rats** *Brain research* **528**:12–20 https://doi.org/10.1016/0006-8993(90)90188-h

59 M'Harzi M., Jarrard L. E (1992) **Effects of medial and lateral septal lesions on acquisition of a place and cue radial maze task** *Behav Brain Res* **49**:159–165 https://doi.org/10.1016/s0166-4328(05)80160-3

60 Wang Y., Romani S., Lustig B., Leonardo A., Pastalkova E (2015) **Theta sequences are essential for internally generated hippocampal firing fields** *Nat Neurosci* **18**:282–288 https://doi.org/10.1038/nn.3904

61 McNaughton N., Ruan M., Woodnorth M. A (2006) **Restoring theta-like rhythmicity in rats restores initial learning in the Morris water maze** *Hippocampus* **16**:1102–1110 https://doi.org/10.1002/hipo.20235

62 Lee D. J., et al. (2013) **Medial septal nucleus theta frequency deep brain stimulation improves spatial working memory after traumatic brain injury** *J Neurotrauma* **30**:131–139 https://doi.org/10.1089/neu.2012.2646

63 Hasselmo M. E., Bodelon C., Wyble B. P (2002) **A proposed function for hippocampal theta rhythm: separate phases of encoding and retrieval enhance reversal of prior learning** *Neural Comput* **14**:793–817 https://doi.org/10.1162/089976602317318965

64 Rutishauser U., Ross I. B., Mamelak A. N., Schuman E. M (2010) **Human memory strength is predicted by theta-frequency phase-locking of single neurons** *Nature* **464**:903–907 https://doi.org/10.1038/nature08860

65 Siegle J. H., Wilson M. A (2014) **Enhancement of encoding and retrieval functions through theta phase-specific manipulation of hippocampus** *Elife* **3** https://doi.org/10.7554/eLife.03061

66 Vandecasteele M., et al. (2014) **Optogenetic activation of septal cholinergic neurons suppresses sharp wave ripples and enhances theta oscillations in the hippocampus** *Proc Natl Acad Sci U S A* **111**:13535–13540 https://doi.org/10.1073/pnas.1411233111

67 Valero M., et al. (2015) **Determinants of different deep and superficial CA1 pyramidal cell dynamics during sharp-wave ripples** *Nat Neurosci* **18**:1281–1290 https://doi.org/10.1038/nn.4074

68 Deuchars J., Thomson A. M (1996) **CA1 pyramid-pyramid connections in rat hippocampus in vitro: dual intracellular recordings with biocytin filling** *Neuroscience* **74**:1009–1018 https://doi.org/10.1016/0306-4522(96)00251-5

69 Caporale N., Dan Y (2008) **Spike timing-dependent plasticity: a Hebbian learning rule** *Annu Rev Neurosci* **31**:25–46 https://doi.org/10.1146/annurev.neuro.31.060407.125639

70 Markram H., Lubke J., Frotscher M., Sakmann B (1997) **Regulation of synaptic efficacy by coincidence of postsynaptic APs and EPSPs** *Science* **275**:213–215 https://doi.org/10.1126/science.275.5297.213

71 Bi G. Q., Poo M. M (1998) **Synaptic modifications in cultured hippocampal neurons: dependence on spike timing, synaptic strength, and postsynaptic cell type** *J Neurosci* **18**:10464–10472 https://doi.org/10.1523/JNEUROSCI.18-24-10464.1998

72 Ali A. B., Deuchars J., Pawelzik H., Thomson A. M (1998) **CA1 pyramidal to basket and bistratified cell EPSPs: dual intracellular recordings in rat hippocampal slices** *J Physiol* **507**:201–217 https://doi.org/10.1111/j.1469-7793.1998.201bu.x

73 Ali A. B., Thomson A. M (1998) **Facilitating pyramid to horizontal oriens-alveus interneurone inputs: dual intracellular recordings in slices of rat hippocampus** *J Physiol* **507**:185–199 https://doi.org/10.1111/j.1469-7793.1998.185bu.x

74 Engel A. K., Konig P., Kreiter A. K., Singer W (1991) **Interhemispheric synchronization of oscillatory neuronal responses in cat visual cortex** *Science* **252**:1177–1179 https://doi.org/10.1126/science.252.5009.1177

75 Alonso J. M., Usrey W. M., Reid R. C (1996) **Precisely correlated firing in cells of the lateral geniculate nucleus** *Nature* **383**:815–819 https://doi.org/10.1038/383815a0

76 Zheng Q., et al. (2019) **Rational Design of Fluorogenic and Spontaneously Blinking Labels for Super-Resolution Imaging** *ACS Cent Sci* **5**:1602–1613 https://doi.org/10.1021/acscentsci.9b00676

Article and author information

En-Li Chen
Institute of Neuroscience, National Yang Ming Chiao Tung University, Taipei, Taiwan, Brain Research Center, National Yang Ming Chiao Tung University, Taipei, Taiwan

Tsai-Wen Chen
Institute of Neuroscience, National Yang Ming Chiao Tung University, Taipei, Taiwan, Brain Research Center, National Yang Ming Chiao Tung University, Taipei, Taiwan

Eric R. Schreiter
Janelia Research Campus, Howard Hughes Medical Institute, Ashburn, VA 20147, USA
ORCID iD: 0000-0002-2864-7469

Bei-Jung Lin
Institute of Neuroscience, National Yang Ming Chiao Tung University, Taipei, Taiwan, Brain Research Center, National Yang Ming Chiao Tung University, Taipei, Taiwan
For correspondence: beijunglin@nycu.edu.tw
ORCID iD: 0000-0002-1755-1664

Copyright

Editors

Reviewing Editor
Laura Colgin
University of Texas at Austin, Austin, United States of America

Senior Editor
Laura Colgin
University of Texas at Austin, Austin, United States of America

Reviewer #1 (Public Review):

Summary:

For many years, there has been extensive electrophysiological research investigating the relationship between local field potential patterns and individual cell spike patterns in the hippocampus. In this study, using state-of-the-art imaging techniques, they examined spike synchrony of hippocampal cells during locomotion and immobility states. In contrast to conventional understanding of the hippocampus, the authors demonstrated that hippocampal place cells exhibit prominent synchronous spikes locked to theta oscillations.

Strengths:

The voltage imaging used in this study is a highly novel method that allows recording not only suprathreshold-level spikes but also subthreshold-level activity. With its high frame rate, it offers time resolution comparable to electrophysiological recordings. Moreover, it enables the visualization of actual cell locations, allowing for the examination of spatial properties (e.g., Figure 4G).

Weaknesses:

There is a notable deviation from several observations obtained through conventional electrophysiological recordings. Particularly, as mentioned below in detail, the considerable differences in baseline firing rates and no observations of ripple-triggered firing patterns raise some concerns about potential artifacts from imaging and analsyis, such as cell toxicity, abnormal excitability, and false detection of spikes. While these findings are intriguing if the validity of these methods is properly proven, accepting the current results as new insights is challenging.

https://doi.org/10.7554/eLife.96718.1.sa2

Reviewer #2 (Public Review):

Summary:

This study employed voltage imaging in the CA1 region of the mouse hippocampus during the exploration of a novel environment. The authors report synchronous activity, involving almost half of the imaged neurons, occurred during periods of immobility. These events did not correlate with SWRs, but instead, occurred during theta oscillations and were phased-locked to the trough of theta. Moreover, pairs of neurons with high synchronization tended to display non-overlapping place fields, leading the authors to suggest these events may play a role in binding a distributed representation of the context.

Strengths:

Technically this is an impressive study, using an emerging approach that allows single-cell resolution voltage imaging in animals, that while head-fixed, can move through a real environment. The paper is written clearly and suggests novel observations about population-level activity in CA1.

Weaknesses:

The evidence provided is weak, with the authors making surprising population-level claims based on a very sparse data set (5 data sets, each with less than 20 neurons simultaneously recorded) acquired with exciting, but less tested technology. Further, while the authors link

these observations to the novelty of the context, both in the title and text, they do not include data from subsequent visits to support this. Detailed comments are below:

(1) My first question for the authors, which is not addressed in the discussion, is why these events have not been observed in the countless extracellular recording experiments conducted in rodent CA1 during the exploration of novel environments. Those data sets often have 10x the neurons simultaneously recording compared to these present data, thus the highly synchronous firing should be very hard to miss. Ideally, the authors could confirm their claims via the analysis of publicly available electrophysiology data sets. Further, the claim of high extra-SWR synchrony is complicated by the observation that their recorded neurons fail to spike during the limited number of SWRs recorded during behavior- again, not agreeing with much of the previous electrophysiological recordings.

(2) The authors posit that these events are linked to the novelty of the context, both in the text, as well as in the title and abstract. However, they do not include any imaging data from subsequent days to demonstrate the failure to see this synchrony in a familiar environment. If these data are available it would strengthen the proposed link to novelty if they were included.

(3) In the discussion the authors begin by speculating the theta present during these synchronous events may be slower type II or attentional theta. This can be supported by demonstrating a frequency shift in the theta recording during these events/immobility versus the theta recording during movement.

(4) The authors mention in the discussion that they image deep-layer PCs in CA1, however, this is not mentioned in the text or methods. They should include data, such as imaging of a slice of a brain post-recording with immunohistochemistry for a layer-specific gene to support this.

https://doi.org/10.7554/eLife.96718.1.sa1

Reviewer #3 (Public Review):

Summary:

In the present manuscript, the authors use a few minutes of voltage imaging of CA1 pyramidal cells in head-fixed mice running on a track while local field potentials (LFPs) are recorded. The authors suggest that synchronous ensembles of neurons are differentially associated with different types of LFP patterns, theta and ripples. The experiments are flawed in that the LFP is not "local" but rather collected in the other side of the brain, and the investigation is flawed due to multiple problems with the point process analyses. The synchrony terminology refers to dozens of milliseconds as opposed to the millisecond timescale referred to in prior work, and the interpretations do not take into account theta phase locking as a simple alternative explanation.

Weaknesses:

The two main messages of the manuscript indicated in the title are not supported by the data. The title gives two messages that relate to CA1 pyramidal neurons in behaving head-fixed mice: (1) synchronous ensembles are associated with theta (2) synchronous ensembles are not associated with ripples.

There are two main methodological problems with the work: (1) experimentally, the theta and ripple signals were recorded using electrophysiology from the opposite hemisphere to the one in which the spiking was monitored. However, both signals exhibit profound differences as a function of location: theta phase changes with the precise location along the

proximo-distal and dorso-ventral axes, and importantly, even reverses with depth. And ripples are often a local phenomenon - independent ripples occur within a fraction of a millimeter within the same hemisphere, let alone different hemispheres. Ripples are very sensitive to the precise depth - 100 micrometers up or down, and only a positive deflection/sharp wave is evident. (2) The analysis of the point process data (spike trains) is entirely flawed. There are many technical issues: complex spikes ("bursts") are not accounted for; differences in spike counts between the various conditions ("locomotion" and "immobility") are not accounted for; the pooling of multiple CCGs assumes independence, whereas even conditional independence cannot be assumed; etc.

Beyond those methodological issues, there are two main interpretational problems: (1) the "synchronous ensembles" may be completely consistent with phase locking to the intracellular theta (as even shown by the authors themselves in some of the supplementary figures). (2) The definition of "synchrony" in the present work is very loose and refers to timescales of 20-30 ms. In previous literature that relates to synchrony of point processes, the timescales discussed are 1-2 ms, and longer timescales are referred to as the "baseline" which is actually removed (using smoothing, jittering, etc.).

https://doi.org/10.7554/eLife.96718.1.sa0

Author response:

> ***Reviewer #1 (Public Review):***
>
> *Summary:*
>
> *For many years, there has been extensive electrophysiological research investigating the relationship between local field potential patterns and individual cell spike patterns in the hippocampus. In this study, using state-of-the-art imaging techniques, they examined spike synchrony of hippocampal cells during locomotion and immobility states. In contrast to conventional understanding of the hippocampus, the authors demonstrated that hippocampal place cells exhibit prominent synchronous spikes locked to theta oscillations.*
>
> *Strengths:*
>
> *The voltage imaging used in this study is a highly novel method that allows recording not only suprathreshold-level spikes but also subthreshold-level activity. With its high frame rate, it offers time resolution comparable to electrophysiological recordings. Moreover, it enables the visualization of actual cell locations, allowing for the examination of spatial properties (e.g., Figure 4G).*

We thank the reviewer for pointing out the technical novelty of this work.

> *Weaknesses:*
>
> *There is a notable deviation from several observations obtained through conventional electrophysiological recordings. Particularly, as mentioned below in detail, the considerable differences in baseline firing rates and no observations of ripple-triggered firing patterns raise some concerns about potential artifacts from imaging and analysis, such as cell toxicity, abnormal excitability, and false detection of spikes. While these findings are intriguing if the validity of these methods is properly proven, accepting the current results as new insights is challenging.*

We appreciate the reviewer's insightful comments regarding the intriguing aspect of our findings. Indeed, the emergence of a novel form of CA1 population synchrony presents exciting implications for hippocampal memory research and beyond.

While we acknowledge the deviations from conventional electrophysiological recordings, we respectfully contend that these differences do not necessarily imply methodological flaws. All experiments and analyses were conducted with meticulous adherence to established standards in the field.

Regarding the observed variations in averaging firing rates, it is important to note the well-documented heterogeneity in CA1 pyramidal neuron firing rates, spanning from 0.01 to 10 Hz, with a skewed distribution toward lower frequencies (Mizuseki et al., 2013). Our exclusion criteria for neurons with low estimated firing rates may have inadvertently biased the selection towards more active neurons. Moreover, prior research has indicated that averaging firing rates tend to increase during exposure to novel environments (Karlsson et al., 2008), and among deep-layer CA1 pyramidal neurons (Mizuseki et al., 2011). Given our recording setup in a highly novel environment and the predominance of deep CA1 pyramidal neurons in our sample, the observed higher averaging firing rates could be influenced by these factors. Considering these points, our mean firing rates (3.2 Hz) are reasonable estimations compared to previously reported values obtained from electrophysiological recordings (2.1 Hz in McHugh et al., 1996 and 2.4-2.6 Hz in Buzsaki et al., 2003).

Regarding concerns about potential cell toxicity, previous studies have shown that Voltron expression and illumination do not significantly alter membrane resistance, membrane capacitance, resting membrane potentials, spike amplitudes, and spike width (see Abdelfattah 2019, Science, Supplementary Figure 11 and 12). In our recordings, imaged neurons exhibit preserved membrane and dendritic morphology during and after experiments (Author response image 1), supporting the absence of significant toxicity.

Author response image 1.

Voltron-expressing neurons exhibit preserved membrane and dendritic morphology. (A) Images of two-photon z-stack maximum intensity projection showing Voltron-expressing neurons taken after voltage image experiments in vivo. (B) Post-hoc histological images of neurons being voltage-imaged.

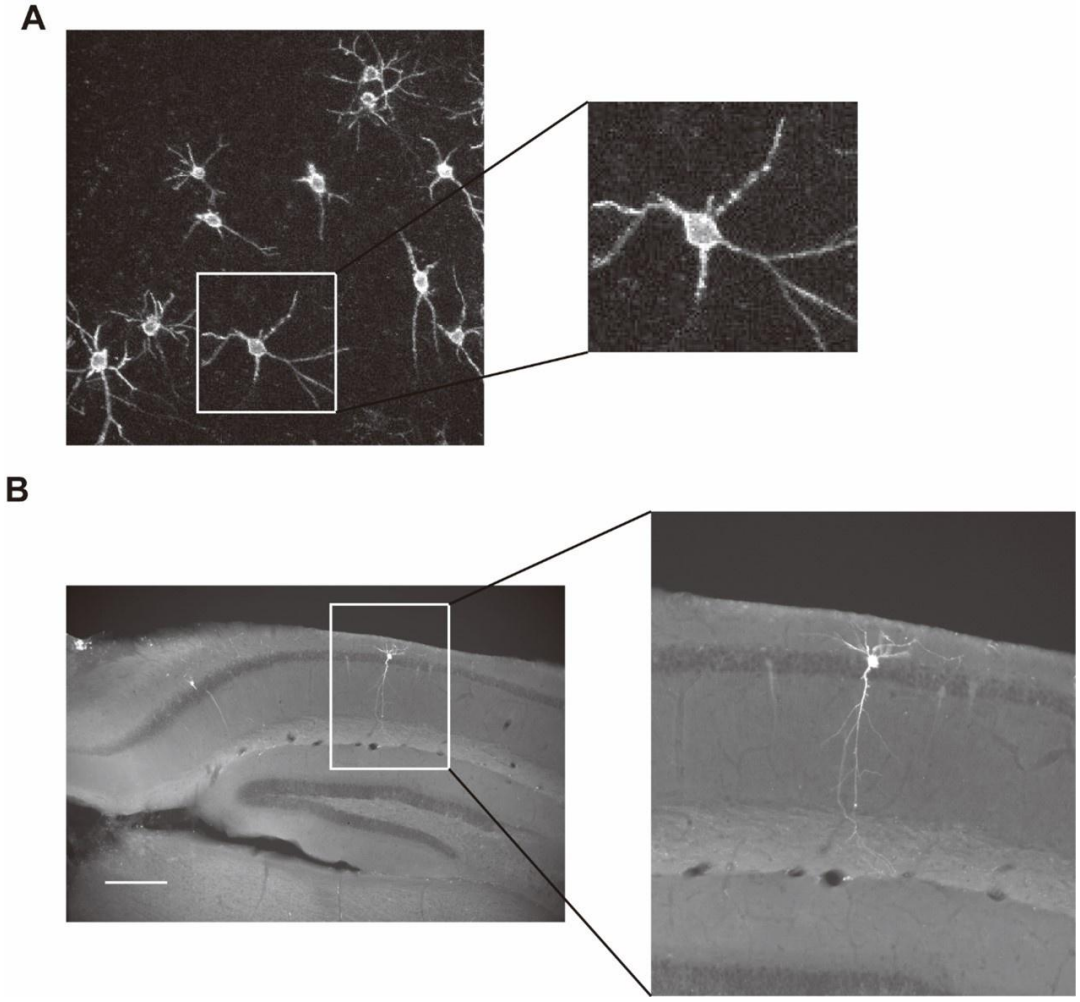

Regarding spike detection, we use validated algorithms (Abdelfattah et al., 2019 and 2023) to ensure robust and reliable detection of spikes. Spiking activity was first separated from slower subthreshold potentials using high-pass filtering. This way, a slow fluorescence increase will not be detected as a spike, even if its amplitude is large. We benchmarked the detection algorithm in computer simulation. The sensitivity and specificity of the algorithm exceed 98% at the level of signal-to-noise ratio of our recordings. While we acknowledge that a small number of spikes, particularly those occurring later in a burst, might be missed due to their smaller amplitudes (as illustrated in Figure 1 and 2 of the manuscript), we anticipate that any missed spikes would lead to a decrease rather than an increase in synchrony between neurons. Overall, we are confident that spike detection is performed in a rigorous and robust manner.

To further strengthen these points, we will include the following in the revision:

(1) Histological images of recorded neurons during and after experiments.

(2) Further details regarding the validation of spike detection algorithms.

(3) Analysis of publicly available electrophysiological datasets.

(4) Discussion regarding the reasons behind the novelty of some of our findings compared to previous observations.

In conclusion, we assert that our experimental and analysis approach upholds rigorous standards. We remain committed to reconciling our findings with previous observations and welcome further scrutiny and engagement from the scientific community to explore the intriguing implications of our findings.

> ***Reviewer #2 (Public Review):***
>
> *Summary:*
>
> *This study employed voltage imaging in the CA1 region of the mouse hippocampus during the exploration of a novel environment. The authors report synchronous activity, involving almost half of the imaged neurons, occurred during periods of immobility. These events did not correlate with SWRs, but instead, occurred during theta oscillations and were phased-locked to the trough of theta. Moreover, pairs of neurons with high synchronization tended to display non-overlapping place fields, leading the authors to suggest these events may play a role in binding a distributed representation of the context.*

We thank the reviewer for a thorough and thoughtful review of our paper.

> *Strengths:*
>
> *Technically this is an impressive study, using an emerging approach that allows single-cell resolution voltage imaging in animals, that while head-fixed, can move through a real environment. The paper is written clearly and suggests novel observations about population-level activity in CA1.*

We thank the reviewer for pointing out the technical strength and the novelty of our observations.

> *Weaknesses:*
>
> *The evidence provided is weak, with the authors making surprising population-level claims based on a very sparse data set (5 data sets, each with less than 20 neurons simultaneously recorded) acquired with exciting, but less tested technology. Further, while the authors link these observations to the novelty of the context, both in the title and text, they do not include data from subsequent visits to support this. Detailed comments are below:*

We understand the reviewer's concerns regarding the size of the dataset. Despite this limitation, it is important to note that synchronous ensembles beyond what could be expected from chance (jittering) were detected in all examined data. In the revision, we plan to add more data, including data from subsequent visits, to further strengthen our findings.

> *(1) My first question for the authors, which is not addressed in the discussion, is why these events have not been observed in the countless extracellular recording experiments conducted in rodent CA1 during the exploration of novel environments. Those data sets often have 10x the neurons simultaneously recording compared to these present data, thus the highly synchronous firing should be very hard to miss. Ideally, the authors could confirm their claims via the analysis of publicly available electrophysiology data sets. Further, the claim of high extra-SWR synchrony is complicated by the observation that their recorded neurons fail to spike during the limited number of SWRs recorded during behavior- again, not agreeing with much of the previous electrophysiological recordings.*

We understand the reviewer's concern. We will examine publicly available electrophysiology datasets to gain further insights into any similarities and differences to our findings. Based on these results, we will discuss why these events have not been previously observed/reported.

> *(2) The authors posit that these events are linked to the novelty of the context, both in the text, as well as in the title and abstract. However, they do not include any imaging data from subsequent days to demonstrate the failure to see this synchrony in a familiar environment. If these data are available it would strengthen the proposed link to novelty if they were included.*

We thank the reviewer's constructive suggestion. We will acquire more datasets from subsequent visits to gain further insights into these synchronous events.

> *1. In the discussion the authors begin by speculating the theta present during these synchronous events may be slower type II or attentional theta. This can be supported by demonstrating a frequency shift in the theta recording during these events/immobility versus the theta recording during movement.*

We thank the reviewer's constructive suggestion. We did demonstrate a frequency shift to a lower frequency in the synchrony-associated theta during immobility than during locomotion (see Fig. 4B, the red vs. blue curves). We will enlarge this panel and specifically refer to it in the corresponding discussion paragraph.

> *(4) The authors mention in the discussion that they image deep-layer PCs in CA1, however, this is not mentioned in the text or methods. They should include data, such as imaging of a slice of a brain post-recording with immunohistochemistry for a layer-specific gene to support this.*

We thank the reviewer's constructive suggestion. We do have images of brain slices post-recordings (Author response image 2). Imaged neurons are clearly located in the deep CA1 pyramidal layer. We will add these images and quantification in the revised manuscript.

Author response image 2.

Imaged neurons are located in the deep pyramidal layer of the dorsal hippocampal CA1 region.

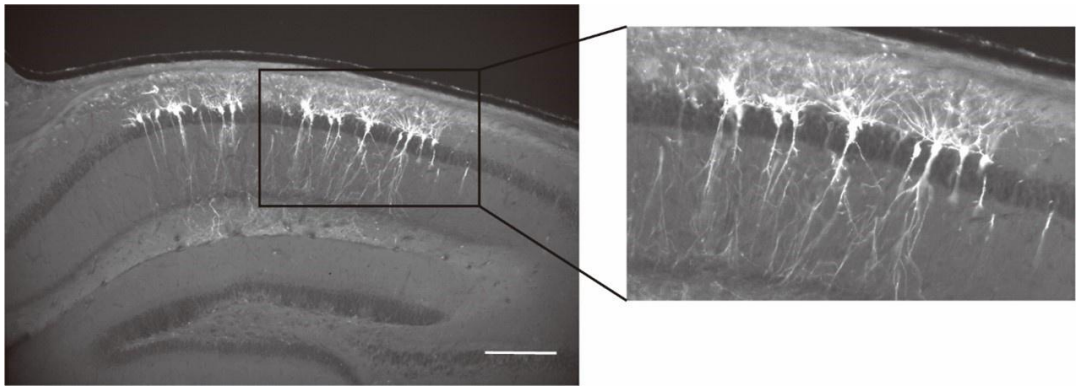

> ***Reviewer #3 (Public Review):***
>
> *Summary:*

> *In the present manuscript, the authors use a few minutes of voltage imaging of CA1 pyramidal cells in head-fixed mice running on a track while local field potentials (LFPs) are recorded. The authors suggest that synchronous ensembles of neurons are differentially associated with different types of LFP patterns, theta and ripples. The experiments are flawed in that the LFP is not "local" but rather collected in the other side of the brain, and the investigation is flawed due to multiple problems with the point process analyses. The synchrony terminology refers to dozens of milliseconds as opposed to the millisecond timescale referred to in prior work, and the interpretations do not take into account theta phase locking as a simple alternative explanation.*

We genuinely appreciate the reviewer's feedback and acknowledge the concerns raised. However, we believe these concerns can be effectively addressed without undermining the validity of our conclusions. With this in mind, we respectfully disagree with the assessment that our experiments and investigation are flawed. Please allow us to address these concerns and offer additional context to support the validity of our study.

> *Weaknesses:*
>
> *The two main messages of the manuscript indicated in the title are not supported by the data. The title gives two messages that relate to CA1 pyramidal neurons in behaving head-fixed mice: (1) synchronous ensembles are associated with theta (2) synchronous ensembles are not associated with ripples.*
>
> *There are two main methodological problems with the work:*
>
> *(1) Experimentally, the theta and ripple signals were recorded using electrophysiology from the opposite hemisphere to the one in which the spiking was monitored. However, both signals exhibit profound differences as a function of location: theta phase changes with the precise location along the proximo-distal and dorso-ventral axes, and importantly, even reverses with depth. And ripples are often a local phenomenon - independent ripples occur within a fraction of a millimeter within the same hemisphere, let alone different hemispheres. Ripples are very sensitive to the precise depth - 100 micrometers up or down, and only a positive deflection/sharp wave is evident.*

We appreciate the reviewer's consideration regarding the collection of LFP from the contralateral hemisphere. While we acknowledge the limitation of this design, we believe that our findings still offer valuable insights into the dynamics of synchronous ensembles. Despite potential variations in theta phases with recording locations and depth, we find that the occurrence and amplitudes of theta oscillations are generally coordinated across hemispheres (Buzsaki et al., Neurosci., 2003). Therefore, the presence of prominent contralateral LFP theta around the times of synchronous ensembles in our study (see Figure 4A of the manuscript) strongly supports our conclusion regarding their association with theta oscillations, despite the collection of LFP from the opposite hemisphere.

In addition, in our manuscript, we specifically mentioned that the "preferred phases" varied from session to session, likely due to the variability of recording locations (see Line 254-256). Therefore, we think that the reviewer's concern regarding theta phase variability has already been addressed in the present manuscript.

Regarding ripple oscillations, while we recognize that they can sometimes occur locally, the majority of ripples occur synchronously in both hemispheres (up to 70%, see Szabo et al., Neuron, 2022; Buzsaki et al., Neurosci., 2003). Therefore, using contralateral LFP to infer ripple occurrence on the ipsilateral side has been a common practice in the field, employed by many studies published in respectable journals (Szabo et al., Neuron, 2022; Terada et al., Nature, 2021; Dudok et al., Neuron, 2021; Geiller et al., Neuron, 2020). Furthermore, our

observation that 446 synchronous ensembles during immobility do not co-occur with contralateral ripples, and the remaining 313 ensembles during locomotion are not associated with ripples, as ripples rarely occur during locomotion. Therefore, our conclusion that synchronous ensembles are not associated with ripple oscillations is supported by data.

> *(2) The analysis of the point process data (spike trains) is entirely flawed. There are many technical issues: complex spikes ("bursts") are not accounted for; differences in spike counts between the various conditions ("locomotion" and "immobility") are not accounted for; the pooling of multiple CCGs assumes independence, whereas even conditional independence cannot be assumed; etc.*

We acknowledge the reviewer's concern regarding spike train analysis. Indeed, complex bursts or different behavioral conditions can lead to differences in spike counts that could potentially affect the detection of synchronous ensembles. However, our jittering procedure (see Line 121-132) is designed to control for the variation of spike counts. Importantly, while the jittered spike trains also contain the same spike count variations, we found 7.8-fold more synchronous events in our data compared to jitter controls (see Figure 1G of the manuscript), indicating that these factors cannot account for the observed synchrony.

To explicitly demonstrate that complex bursts cannot account for the observed synchrony, we have performed additional analysis to remove all latter spikes in bursts and only count the single and the first spikes of bursts. Importantly, we found that this procedure did not change the rate and size of synchronous ensembles, nor did it significantly alter the grand-average CCG (see Author response image 3). The results of this analysis explicitly rule out a significant effect of complex spikes on the analysis of synchronous ensembles.

Author response image 3.

Population synchrony remains after the removal of spikes in bursts. (A) The grand-average cross correlogram (CCG) was calculated using spike trains without latter spikes in bursts. The gray line represents the mean grand average CCG between reference cells and randomly selected cells from different sessions. (B) Pairwise comparison of the event rates of population synchrony between spike trains containing all spikes and spike trains without latter spikes in bursts. Bar heights indicate group means (n=10 segments, p=0.036, Wilcoxon signed-rank test). (C) Histogram of the ensemble sizes as percentages of cells participating in the synchronous ensembles.

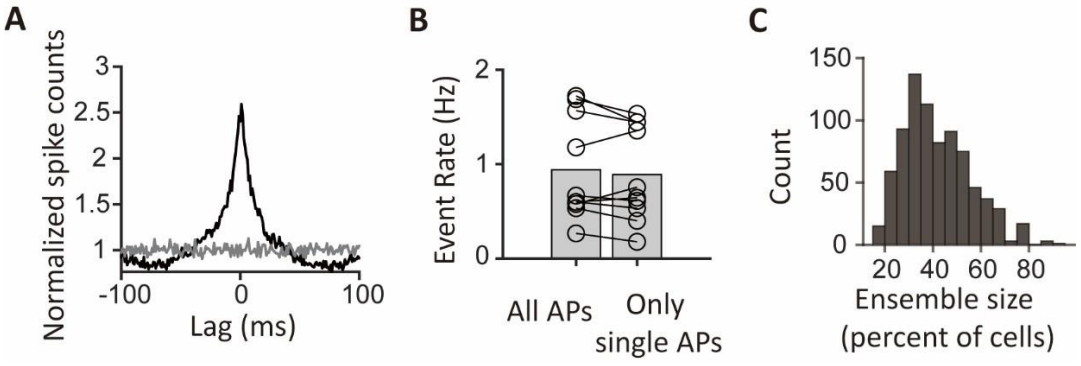

> *Beyond those methodological issues, there are two main interpretational problems: (1) the "synchronous ensembles" may be completely consistent with phase locking to the intracellular theta (as even shown by the authors themselves in some of the supplementary figures).*

We agree with the reviewer that the synchronous ensembles are indeed consistent with theta phase locking. However, it is important to note that theta phase locking alone does not necessarily imply population synchrony. In fact, theta phase locking has been shown to "reduce" population synchrony in a previous study (Mizuseki et al., 2014, Phil. Trans. R. Soc. B.). Thus, the presence of theta phase locking cannot be taken as a simple alternative explanation of the synchronous ensembles.

To directly assess the contribution of theta phase locking to synchronous ensembles, we have performed a new analysis to randomize the specific theta cycles in which neurons spike, while keeping the spike phases constant. This manipulation disrupts spike co-occurrence while preserving theta phase locking, allowing us to test whether theta phase locking alone can explain the population synchrony, or whether spike co-occurrence in specific cycles is required. The grand-average CCG shows a much smaller peak compared to the original peak (Author response image 4A). Moreover, synchronous event rates show a 4.5-fold decrease in the randomized data compared to the original event rates (Author response image 4B). Thus, the new analysis reveals theta phase locking alone cannot account for the population synchrony.

Author response image 4.

Drastic reduction of population synchrony by randomizing spikes to other theta cycles while preserving the phases. (A) The grand-average cross correlogram (CCG) was calculated using original spike trains (black) and randomized spike trains where theta phases of the spikes are kept the same but spike timings were randomly moved to other theta cycles (red). (B) Pairwise comparison of the event rates of population synchrony between the original spike trains and randomized spike trains (n=10 segments, p=0.002, Wilcoxon signed-rank test). Bar heights indicate group means. ** $p<0.01$

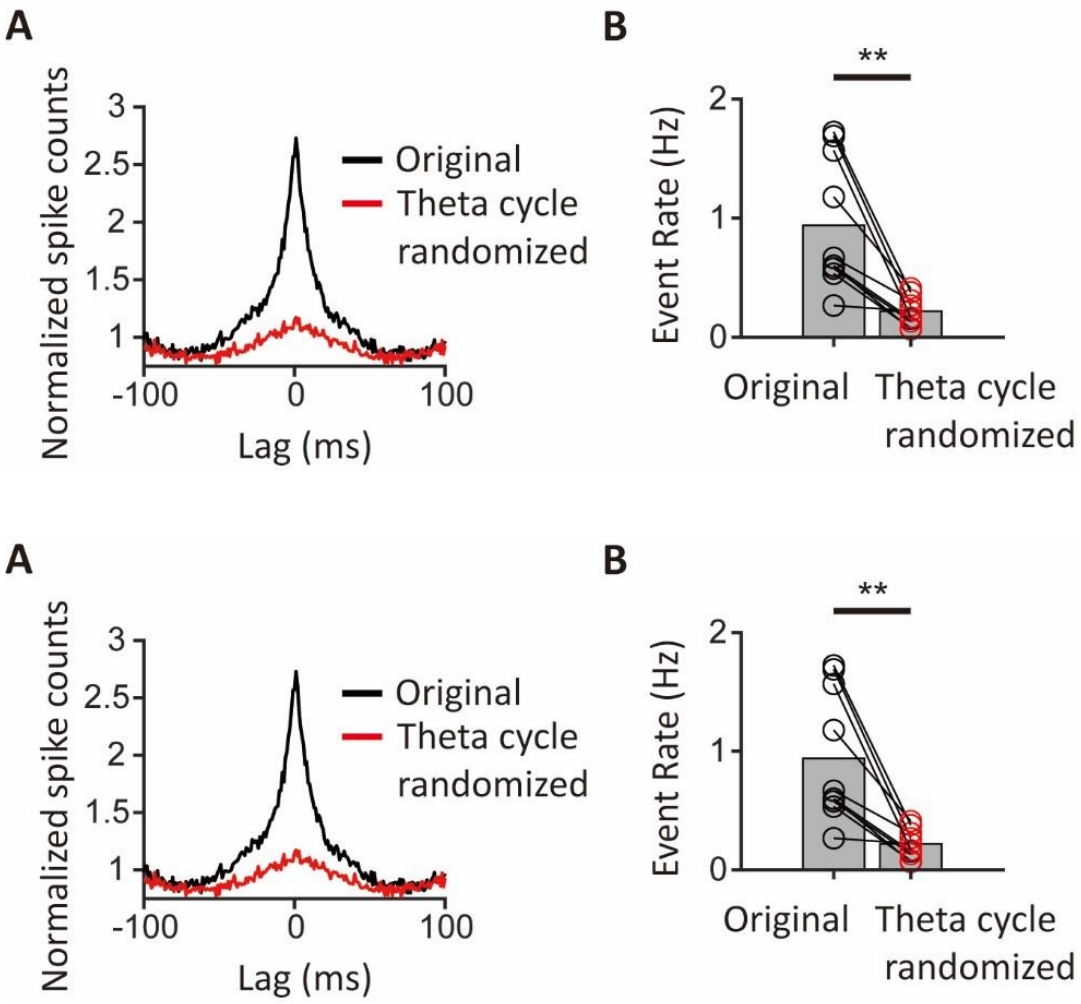

> *(2) The definition of "synchrony" in the present work is very loose and refers to timescales of 20-30 ms. In previous literature that relates to synchrony of point processes, the timescales discussed are 1-2 ms, and longer timescales are referred to as the "baseline" which is actually removed (using smoothing, jittering, etc.).*

Regarding the timescale of synchronous ensembles, we acknowledge that it varies considerably across studies and cell types. However, it is important to note that a timescale of dozens, or even hundreds of milliseconds is common for synchrony terminology in CA1 pyramidal neurons (see Csicsvari et al., Neuron, 2000; Harris et al., Science, 2003; Malvache et al., Science, 2016; Yagi et al., Cell Reports, 2023). In fact, a timescale of 20-30 ms is considered particularly important for information transmission and storage in CA1, as it matches the membrane time constant of pyramidal neurons, the period of hippocampal gamma oscillations, and the time window for synaptic plasticity. Therefore, we believe that this timescale is relevant and in line with established practices in the field.